AN ABSTRACT OF THE THESIS OF

ALAN LEE FAHRENBRUCH for the M.S. in Physics
(Name of student) (Degree) (Major)

presented on November 28, 1967
(Date)

Title: PHOTOELECTRIC PROPERTIES OF EVAPORATED ANTIMONY FILMS AS A FUNCTION OF FILM THICKNESS

Abstract approved: Redacted for privacy
James J. Brady

The total photoemission and optical properties of thin films of antimony up to 320Å in thickness were studied as a function of film thickness in light emergent geometry. The films were evaporated onto a quartz substrate from a tantalum oven using 99.999% pure antimony and film thickness measurements were obtained from optical transmission data. Using a vibrating capacitor technique, the variation in average work function with film thickness was measured by comparison with a standard gold film. At a thickness of approximately 165Å the film rapidly became conductive with an assumed change from amorphous to crystalline structure. Photoemission from films in the 150Å - 350Å thickness range was correlated with electron mean-free-path and optical transmission data.

PHOTOELECTRIC PROPERTIES OF EVAPORATED ANTIMONY FILMS AS A FUNCTION OF FILM THICKNESS

by

ALAN LEE FAHRENBRUCH

A THESIS

SUBMITTED TO

OREGON STATE UNIVERSITY

IN PARTIAL FULFILLMENT OF
THE REQUIREMENT FOR THE

DEGREE OF

MASTER OF SCIENCE

JUNE, 1969

APPROVED:

Redacted for privacy

Professor of Physics in Charge of Thesis

Redacted for privacy

Chairman of Department of Physics

Redacted for privacy

Dean of Graduate School

Thesis presented on [illegible]

Typed by Iris Hansen

ACKNOWLEDGEMENT

The author wishes to express his sincere appreciation to Dr. J. J. Brady who suggested the problem and offered much help and advice toward its completion. He also wishes to extend his gratitude to Dr. E. A. Yunker whose encouragement made the difficult experimental work less formidable.

TABLE OF CONTENTS

TABLE OF FIGURES

PHOTOELECTRIC PROPERTIES OF EVAPORATED ANTIMONY FILMS AS A FUNCTION OF THICKNESS

I. INTRODUCTION

The discovery and explanation of the photoelectric effect stands out not only as one of the most important verifications of the quantum theory but as a tribute to the persistence and determination of the early physicists. Today the field remains a broad and penetrating study in its own right as well as an increasingly valuable tool in the investigation of electronic band structure in solids, electron collision phenomena, and surface physics.

Since the first evidences of the photoelectric effect were noticed in 1887 when Hertz found lowered sparking potentials between illuminated spheres, hundreds of workers have studied its effects and ramifications. The most notable, of course, was A. Einstein (10) whose successful explanation of the linear relation between photoelectron energy and incident light frequency set the physics world agog with its revolutionary assumptions.

Suppose we shine some light on a metallic conductor in a vacuum. By the total absorption of a single photon of radiation, an electron may acquire kinetic energy equal to the photon energy and then proceed to lose this energy by various types of collisions and in overcoming the potential barrier at the metal surface. Using the Fermi-Dirac distribution of initial electron energies as a starting point with semi-quantum-mechanical models of the mechanics of excitation and potential barrier transmission, various workers developed theories

of the process of emission. These seemingly crude models gave remarkable agreement with experiment. Among the most successful were the theories of Fowler (11), Ives (14), and DuBridge (8). These theories relate the energy and spectral distributions of the electrons to the emitter temperature near the threshold frequency.

The complicating effects of a variety of collision phenomena, the special potentials within and at the boundary of the metal as well as the state of polarization and monochromaticity of the light, and the structure of real surfaces demand the sophisticated techniques of a fully quantum mechanical treatment.

Examination of the special properties of the photoelectric effect from thin films is attractive since the problem is somewhat simplified by control of a spatial dimension of the same order as the electron mean free path, optical wavelengths, and optical absorption length. For the long history of thin film photoelectric research see the book by Hughes and DuBridge (13). Beyond this, thin film techniques are particularly important in their application to closely related electro-optic and electromagnetic phenomena.

Because of the necessarily limited theoretical scope of this paper the problem was approached rather cautiously from a semiclassical point of view. Thus, an emphasis has been placed on the development of certain experimental techniques for the study of photoelectric properties in ultra pure thin metal films. In particular these include:

1) Control of film thickness, temperature, and rate of film deposition.

2) The measurement of optical film transmission by a sensitive double pass method.

3) Determinations of the external work function, photoemission energy distribution and threshold, and the total photocurrent as a function of thickness.

4) Monitoring the film's optical properties at photoemission wavelengths.

5) Qualitative measurement of the film's resistivity obtained by a parallel plate capacitance technique.

II. THEORY

INTRODUCTION

To get an overall view let us review first an elementary theory of photoemission from conducting solids.

Einstein, in his 1905 paper (10), proposed that under proper conditions an electron could totally absorb a single quantum of radiant energy which appeared as an increase in the kinetic energy of the electron. If the electron was initially in the interior of a metallic conductor this added kinetic energy might be sufficient to enable the electron to escape the potential barrier at the metal surface and be detected.

Later it was shown that the photon-electron interaction must take place in the field of a third body such as a nucleus, crystal lattice, or the surface potential field to conserve momentum. This can be shown intuitively by a classical inequality or more precisely by a quantum mechanical analysis of the interaction. Since we will use a semi-classical approach in discussing the effect in terms of the free-electron theory of metals we will assume for this discussion that the surface potential field enables momentum to be conserved but claims a negligible portion of the photon's energy.

ELEMENTARY THEORY -

THE ELECTRON ENERGY DISTRIBUTION

In most theories of photoemission it is a well founded and much used assumption that the energy distribution of electrons in a metal before interaction is isotropic and is given by the Fermi-Dirac statistics:

$$n(E)dE = \frac{8\pi(2m^3)^{\frac{1}{2}} E^{\frac{1}{2}}dE}{h^3 \exp[(E - E_f)/kT] + 1} \qquad (1)$$

where the usual symbolism holds and E_f is a constant called the Fermi energy. In Figure 1a, n(E) is shown for T = 0°K and 300°K. It is quite evident that the influence of temperature is strong only at higher energies, but these are the very electrons which are available for photoemission.

If we choose to excite an electron with initial energy E_f whose velocity is directed normal to the metal surface both before and after interaction with the photon, Einstein's equation applies to relate the external energy (E_x) of the emitted electron with the height of the surface potential barrier (ϕe):

$$h\nu - \phi e = \frac{1}{2} m_e u_x^2 = E_x \qquad (2)$$

This relationship is expressed graphically in Figure 1b.

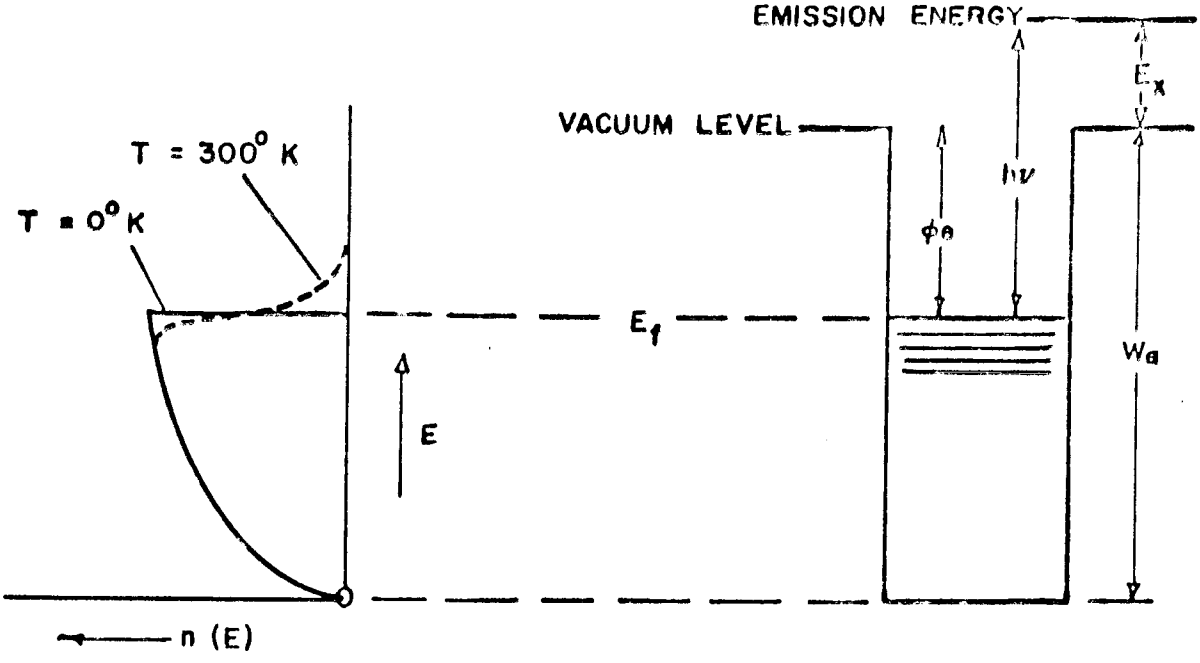

FIGURE 1a. FERMI-DIRAC DISTRIBUTION (Properties at 300° K are exaggerated)

FIGURE 1b. ENERGY LEVEL DIAGRAM

Since the work function, ϕ, is defined by $\phi e = W_a - E_f$ (where W_a is the total height of the potential barrier) at T = 0°K the threshold frequency, $\nu_o = \frac{\phi e}{h}$ (which is the lowest light frequency capable of causing photoemission) is precisely defined only at 0°K. At any higher temperature the number of electrons per energy interval tends to zero asymtotically with increasing E. For the frequencies of light commonly obtainable experimentally the electrons available for photoemission lie in a rather narrow band at the high end of the distribution where temperature dependence is strong.

Experimentally it is usual to determine the energy distribution of the emitted electron by adjusting an external retarding field so that only those electrons with energy eV_R will reach the collector (V_R = collector - emitter potential difference). If the resulting curve relating current and retarding voltage is differentiated an energy distribution curve can be obtained (see Figure 2 for example). Proper attention must be given to geometrical factors of course.

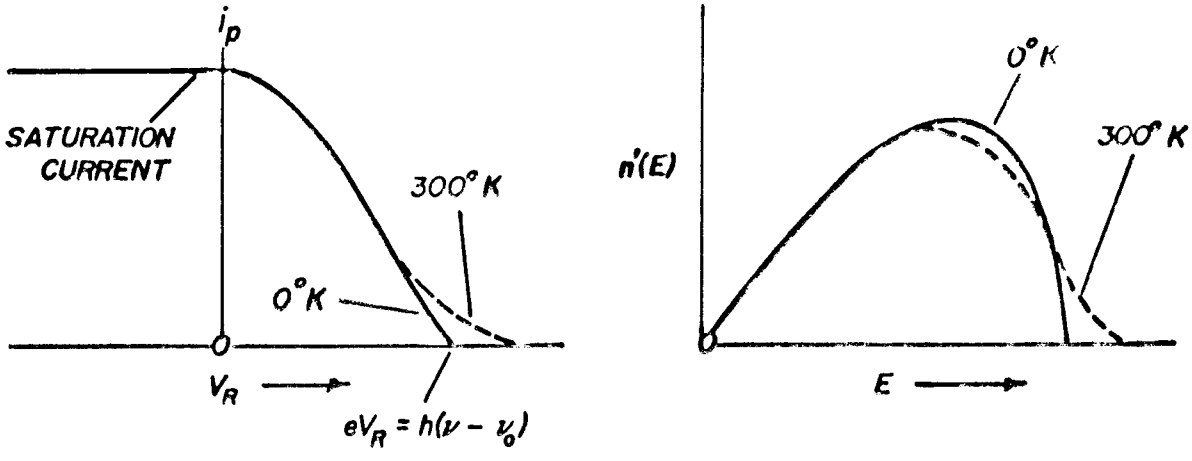

Photocurrent Versus Retarding Potential **Energy Distribution**

(Properties at 300°K are exaggerated)

FIGURE 2. EXPERIMENTAL PHOTOEMISSION CURVES

Parallel plate geometry will yield a distribution of normal energies but for a total energy distribution a concentric sphere arrangement is required.

Let us hypothesize a function, F, which completely specifies the numbers and velocities of the emitted electrons. Then F is a function of (a) the intensity, direction of incidence, state of polarization, and frequency of the incident light, and (b) the work function and

Fermi energy of the metal as well as its temperature and microscopic structure.

Letting all other variables be constant then:

$$dn = F(\nu, \vec{u}, T)d\nu d\vec{u} \tag{3}$$

Integration over the electron velocity, $\vec{u}$, gives a spectral distribution while integration with respect to the light frequency, ν, gives a velocity distribution.

Attempts to derive such expressions have a long history but none were really successful until Sommerfeld's free electron theory in 1927 gave the needed basis. Notable theories were advanced by Richardson[1], Nordheim, Wentzel, Fröhlich, and Tamm and Schubin. The most successful and generally useful of the semiclassical theories were those of Fowler (11) and DuBridge (8). Here we call semiclassical theories those in which the excitation mechanism is not treated as a wave mechanical interaction but as a simple addition of kinetic energy to the electron. These theories used quantum mechanical treatments of the excited electron's barrier penetration however. The theory of DuBridge for parallel plate geometry will be used for analysis of the data of this work.

---

1. Richardson's theory relates total emission to emitter temperature and is based on thermodynamic arguments. It was derived before 1927 and was substantiated by the Sommerfeld theory. These theories are comparatively described in reference 13, page 195.

THE FOWLER-DUBRIDGE THEORY

Fowler's intent was to predict the photo-current, I_p, as a function of ν and T in order to obtain accurate values of ν_o at $T \gg 0^oK$. DuBridge then extended the treatment to make use of measured retarding potential-photocurrent curves at constant ν and T to obtain the same information. (We will discuss the theory of Fowler as modified by DuBridge.)

In outline the method consists of:

1) Expressing the distribution of initial electron velocities, u_o, using the Fermi-Dirac statistics.
2) Computing the probability, $P(\nu, u_o)$, that an electron will absorb a photon.
3) Writing the normal velocity distribution for the flux of electrons to the metal surface where their new energy is given by

$$\frac{mu^2}{2} = h\nu + \frac{mu_o^2}{2} \qquad (4)$$

4) Multiplying this by the transmission coefficient, $D(E_n, \nu_o, W_a, S)$, for the boundary (where S includes shape factors for the boundary and E_n is the portion of the electron's energy directed normal to the boundary).
5) Integrating the result over all values of normal energy to obtain the desired spectral distribution.

Fowler and DuBridge made the following simplifying assumptions which are reasonable for the experimental range of $\nu \lesssim 1.5\ \nu_o$:

(a) The free electron theory holds within the metal with no potential variation save at the boundary.

(b) The range of initial energies is within a few percent of E_f so any probability factors P which depend on a small power of ν will be considered constant.

(c) Factors in $(\nu - \nu_o)$ will make factors in (ν) unimportant.

(d) Assume that
$$D = 1 \quad \text{for} \quad E_n + h\nu \geq W_a$$
$$D = 0 \quad \text{for} \quad E_n + h\nu < W_a \qquad (5)$$

(Although this assumption is actually quite good, it deserves later discussion).

(e) Implicitly assumed are a smooth surface from which the electrons escape and that they suffer no collisions within the metal.

Then N_a, the number of electrons available for emission (which is proportional to emission current since P is constant), can be obtained by integration of $n(E_n)$, the number of electrons emerging with normal energy E_n. (N_a is the number of electrons per unit time per unit area.)

$$N_a = \int_{W_a - h\nu}^{\infty} n(E_n)\,dE_n \qquad (6)$$

$$N_a = \frac{4\pi mkT}{h^3} \int_{W_a - h\nu}^{\infty} \mathrm{Ln}\left[1 + \exp \frac{(E_f - E_n)}{kT}\right] dE_n \qquad (7)$$

This may be integrated to yield:

$$N_a[T, \nu, (E_f - W_a)] = \frac{4\pi mk^2T^2}{h} \phi(x) \qquad (8)$$

where

$$x = \frac{E_f - (W_a - h\nu)}{kT}$$

and

$$\phi(x) = g(x) \qquad \text{for} \quad x \leq 0$$

$$\phi(x) = \frac{x^2}{2} + \frac{\pi^2}{6} - g(-x) \qquad \text{for} \quad x \geq 0$$

$$g(x) = [e^x - \frac{e^{2x}}{2^2} + \frac{e^{3x}}{3^2} - \ldots]$$

Then if we let α = the probability of an electron absorption of a photon we expect

$$I_p = \alpha AT^2\phi(x) \qquad (9)$$

for the saturation current. (A includes all constant factors).[2]

Implicit in this derivation is the assumption that the entire energy of the interacting photon will be added in a direction normal to the photoemitting surface. This is a good approximation for this energy range--see page 95. Also implied is that the effect is a surface phenomenon since we considered the flux of unexcited electrons to the surface where we selected those of appropriate energy as being available for photoemission.

---

2. It is of interest to note that if $\nu = 0$ Equation (9) reduces to the Richardson Equation with the same constant A.

At absolute zero Equation (9) reduces to:

$$I_p = 0 \quad h\nu \leq (W_a - E_f)$$

$$I_p = \frac{1}{2}\frac{\alpha A}{k^2}[h\nu - (W_a - E_f)]^2 \quad \text{for} \quad (W_a - E_f) \leq h\nu \tag{10}$$

Equation (10) represents a parabola whose vertex intersects the axis at

$$\nu = \frac{W_a - E_f}{h} = \nu_o \tag{11}$$

which is just the apparent threshold we sought. Although ν_o does not exist as a sharply defined threshold at $T > 0^oK$ it is convenient to define it as a characteristic frequency by Equation (11). (Also $x = 0$ here.)

Fowler devised a beautifully ingenious graphical method by which ν_o could be found easily be rewriting Equation (8):

$$\text{Ln}\frac{I_p}{T^2} = B + \Phi(x) \tag{12}$$

Since B is a constant independent of ν and T and $\Phi(x) = \text{Ln}\phi(x)$ is a universal function of x (the same for all metals) any experimental curve should be superposable on the theoretical curve by simple translation. If $\text{Ln}(I/T^2)$ is plotted against $\frac{h\nu}{kT}$ the horizontal translation will give ν_o. Experimental agreement with the theory is very good to photon energies as much as 1.3 volts from the threshold.

The DuBridge modification of the Fowler theory is based on the assumption that the external electric field is the same in its effect as the surface potential barrier. Thus if the total potential barrier is W_a we can write for parallel plate geometry

$$W_a' = W_a + V_r e \tag{13}$$

where W_a' is a new, effective total potential barrier and V_r is the external retarding potential. Then the expression for the flux of electrons to the photoemissive surface with energy sufficient to reach the collector becomes

$$N'(V) = \int_{W_a + V_r e - h\nu}^{\infty} n(E_n) dE_n \tag{14}$$

Integration of Equation (14) yields a form like Equation (8) except that x is replaced everywhere by x':

$$x' = \frac{h\nu - (W_a + V_r e - E_f)}{kT} = \frac{(V_m - V_r)e}{kT} \tag{15}$$

(Here V_m corresponds to the threshold on the current-voltage curve at $0^{\circ}K$.) Then the rate at which electrons reach the collector is given by

$$N_c(V_r) = \left[\frac{4\pi mkT^2}{h} \phi(x')\right] \tag{16}$$

The electron energy distribution (normally obtained from the experimental $I_p - V_r$ curve by differentiation) is the differential of Equation (16):

$$n(V_r) = \frac{4\pi\, mkT}{h^3} \operatorname{Ln} \left\{ 1 + \exp\left[\frac{E_f - W_a + V_r e - h\nu}{kT}\right]\right\} \tag{17}$$

The graphical analysis of Fowler can be used unchanged except for inclusion of the variable V_r. So far the assumptions are as before with the additional assumption that the W_a' potential barrier's effect is the same as that corresponding to W_a.

The Fowler-DuBridge theory for parallel plate geometry given above looks good experimentally especially near V_m where the barrier transmission assumption should hold more exactly.

Fowler and DuBridge go on to derive similar but more general expressions for the concentric sphere geometry where the total energy distribution of the electron is desired. In this their assumption is that the velocity acquired by the electrons from the photo excitation is in the same direction as the electron's original velocity. (The original velocities are isotropic.) This theory gives the normal energy result as a special case. An experimental verification of the concentric sphere theory for the special case of thin films was made by Brady (4) who found good agreement for $\tau > 3$ or 4 atomic layers.

THE SURFACE POTENTIAL BARRIER

Since the transmission coefficient for the potential barrier is a function of its shape and height as well as the electron energy it will be of interest to further discuss this point. The simplest assumption of course is that of the rectangular barrier for which D can be readily calculated. (See Figure 3a.) It will be observed that for $E_n \approx W_a$, D is a rapid function of E_n. Perhaps a more realistic model is the image field barrier for which Nordheim (20) made calculations indicating

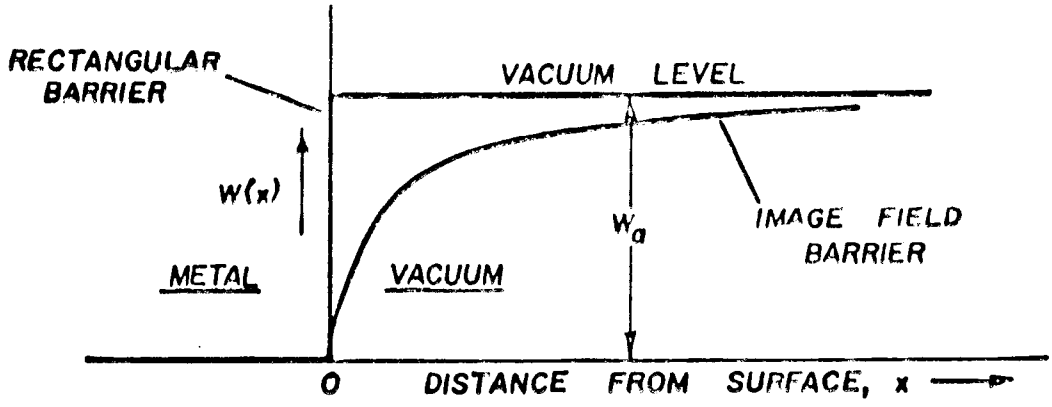

FIGURE 3a. SURFACE POTENTIAL BARRIER MODELS

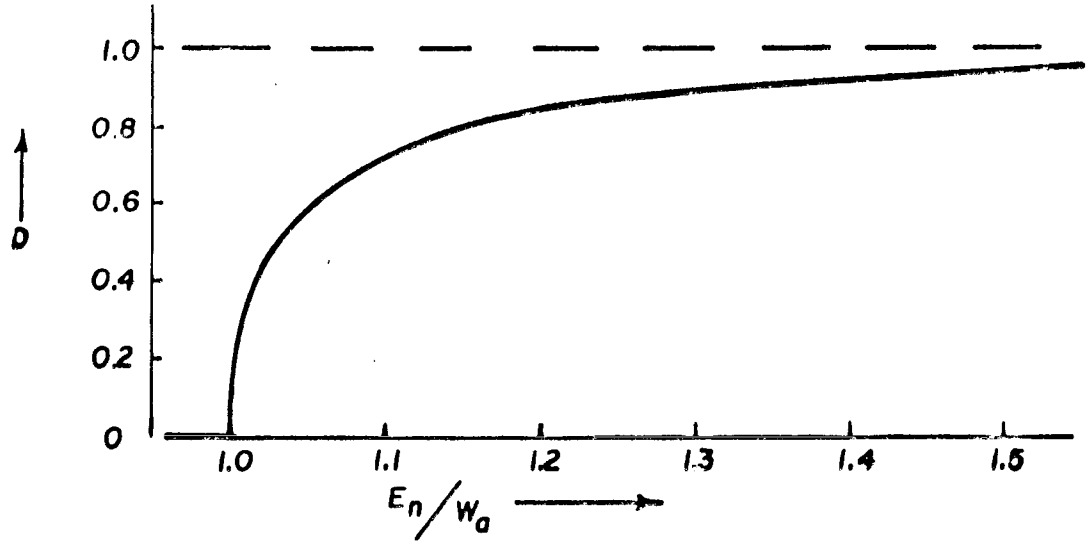

FIGURE 3b. RECTANGULAR BARRIER TRANSMISSION COEFFICIENT

$D = 0.93$ for $E_n = W_a$ (see Figure 3b). More complex barrier shapes give rise to resonance penetration with one or several maxima in the $D(E_n)$ relation. Indeed the most simple deviation from the simple step function model introduces enormous complications as the number of adjustable parameters is increased.

The model assumed for the Fowler-DuBridge theory ($D = 0, E_n < W_a$; $D = 1, E_n \geq W_a$) seems quite satisfactory considering the fact that we

are dealing with frequencies sufficiently removed from the threshold to insure that $D \approx 1$. This is especially true in view of Nordheim's result.[3] In the DuBridge modification the retarding field extends the step barrier but again the major portion of the current which we are analyzing consists of electrons for which $E_n-(W_a + V_r)$ is large enough to make $D \approx 1$.

It is obvious that the development of a complete theory of photoemission critically depends on a satisfactory specification of the surface potential barrier. This is especially true when one considers the actual three dimensional configuration of a real metal surface (17). The periodic potential conditions within the metal influence the excitation process and thus a complete theory must include consideration of a volume photoeffect.

THE THIN FILM EFFECT

After the electron has been excited within a bulk material it may suffer certain collisions on its way to the surface. These include electron-electron and electron-lattice collisions (elastic and inelastic) in a regular crystalline conducting solid. If the solid is of amorphous character or exists as a thin film, collisions involving the surface potential barrier become important. Two modern, comprehensive articles by Bergland and Spicer are recommended (2, 3).

---

3. However, if we are measuring ν_o by actually varying ν, the value of D becomes quite important for $E_n \approx W_a$.

Since specific collision theory is beyond the scope of this paper we will speak only of a "total average mean free path," λ_e, which presumably would be chiefly due to inelastic electron-lattice collisions. We will assume that λ_e is independent of electron energy over our range and that the electrons do not have sufficient energy to escape after one collision.

The depth from which electrons are emitted is a most important aspect of the problem which must be considered in detail in this connection. It is the assumption of this paper that emission near the threshold energy is a surface process taking place within the portion of the surface potential barrier for which the gradient is relatively large. Although there are potential conditions within the metal which permit photon-electron interaction it is believed that the threshold for this type of excitation is higher and that yields are smaller (15).

Since a portion of the electrons will always be emitted without collision the straightforward determination of threshold (near $T = 0^{\circ}K$) will not be affected although the energy distribution may be. Brady (4) has found that the energy distribution from potassium films on a silver backing is not appreciable affected by film thickness (for films greater than three atoms thick) in light incident geometry. Experimental data was a good fit to the Fowler-DuBridge theory.

By the investigation of thin film emitters the assumptions concerning electron mean free path and surface versus volume photoemission may be explored providing something of the structure and optical properties of the film material are known.

III. EXPERIMENTAL APPARATUS

In the construction of apparatus the following measurements were considered:

Film thickness
Film temperature
Photocurrent
Work function
Optical transmission and reflection
Illumination quality and intensity
Metal purity and deposition rate

In order to design a proper environment the experiment was divided into five general subsystems each imposing particular requirements on the system as a whole. There are outlined below:

Optics. To measure the transmission and reflection coefficients of the film in vacuo at two distinct wavelengths an optical system was designed which utilized a double pass of light through the film. This made possible the use of a single quartz window and a single, rigidly mounted detector. Since optical transmission was the principal means of film thickness determination, accuracy of this system was a most important consideration. The same system supplied a beam of ultraviolet light of monitored intensity for photoemission.

Metal Source. After exhaustive experimental work a shutter-controlled molecular beam from a radio-frequency induction heated oven was found to be the best source under consideration of purity, ease of control, and reliability.

Photocurrent Measurement. Although the use of a direct-reading vibrating reed electrometer simplified the measurement of the minute photocurrent (10^{-15} to 10^{-13} amps.) there were numerous problems involving shielding and stability.

Contact Potential Measurement. A freshly evaporated gold film was used as a work function reference with a vibrating capacitor technique for measurement of variations in work function of the film. Inter-electrode capacitances and an approximate measure of film resistivity were also obtained with this system.

General Experimental Set-up. The remaining considerations such as substrate temperature control, production of ultra-high vacuum conditions, and the external electrical circuits are discussed here.

With this outline as an introduction each system will be discussed with reference to theory, design criteria, and the experimental problems of the final configuration. Photos of the experimental layout and a general schematic follow (Figures 4, 5, 6 and 7).

OPTICAL SYSTEM

In a sense this experimental method was made possible by the work of G. A. Condas at LRL (6) who related optical transmission and surface density of similar high-purity antimony films and made it practical to use this method of film thickness determination.

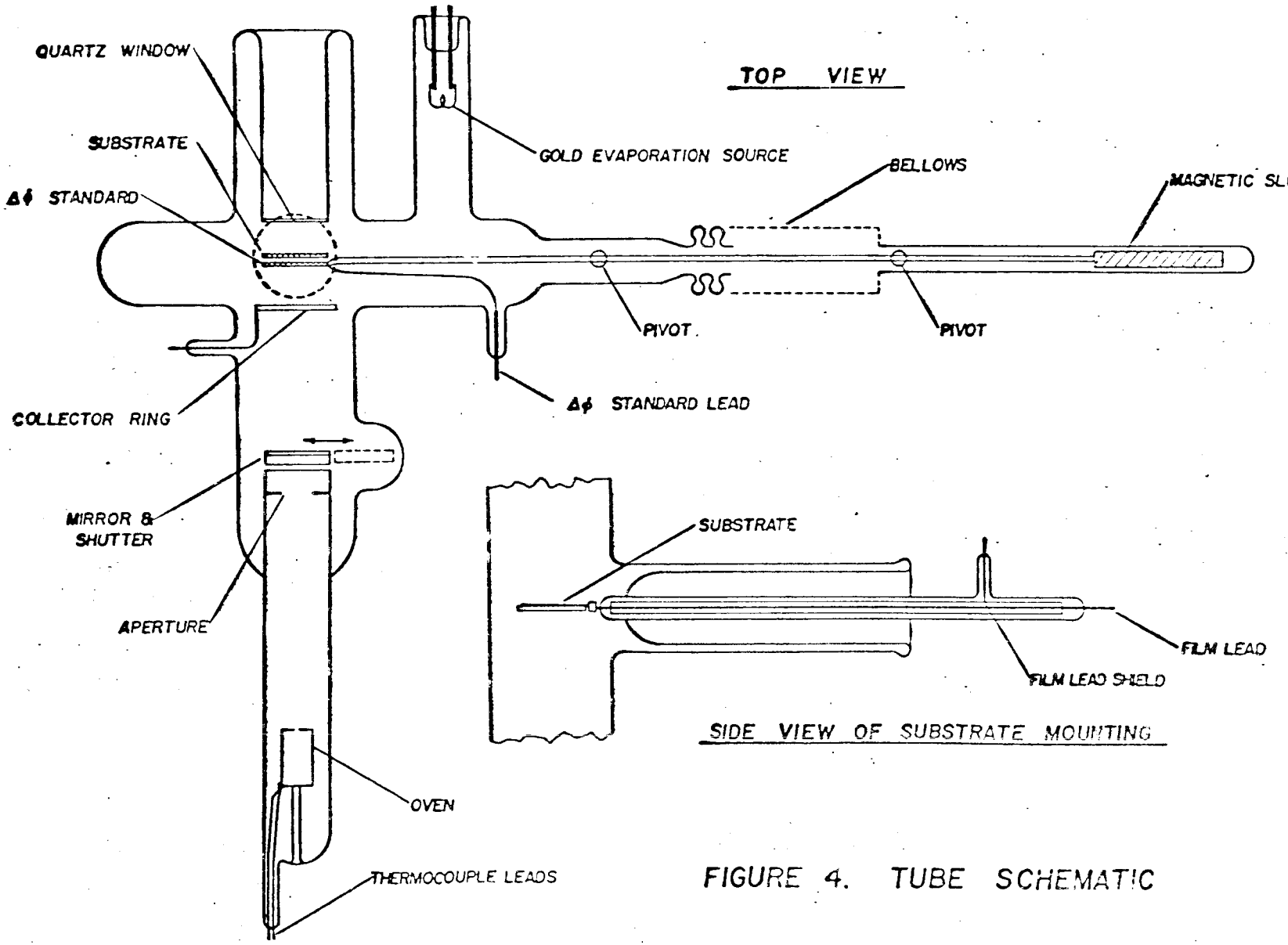

FIGURE 4. TUBE SCHEMATIC

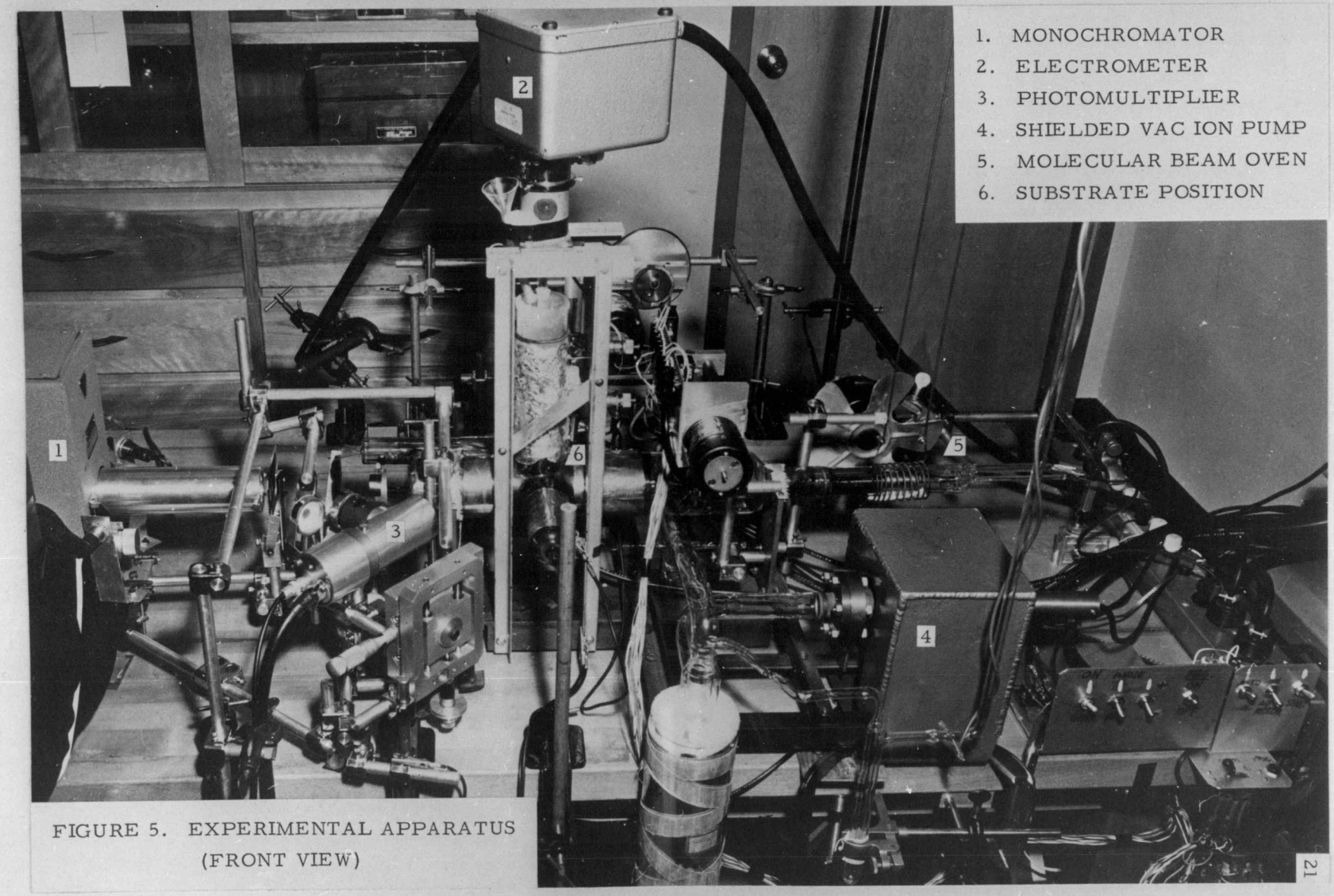

FIGURE 5. EXPERIMENTAL APPARATUS
(FRONT VIEW)

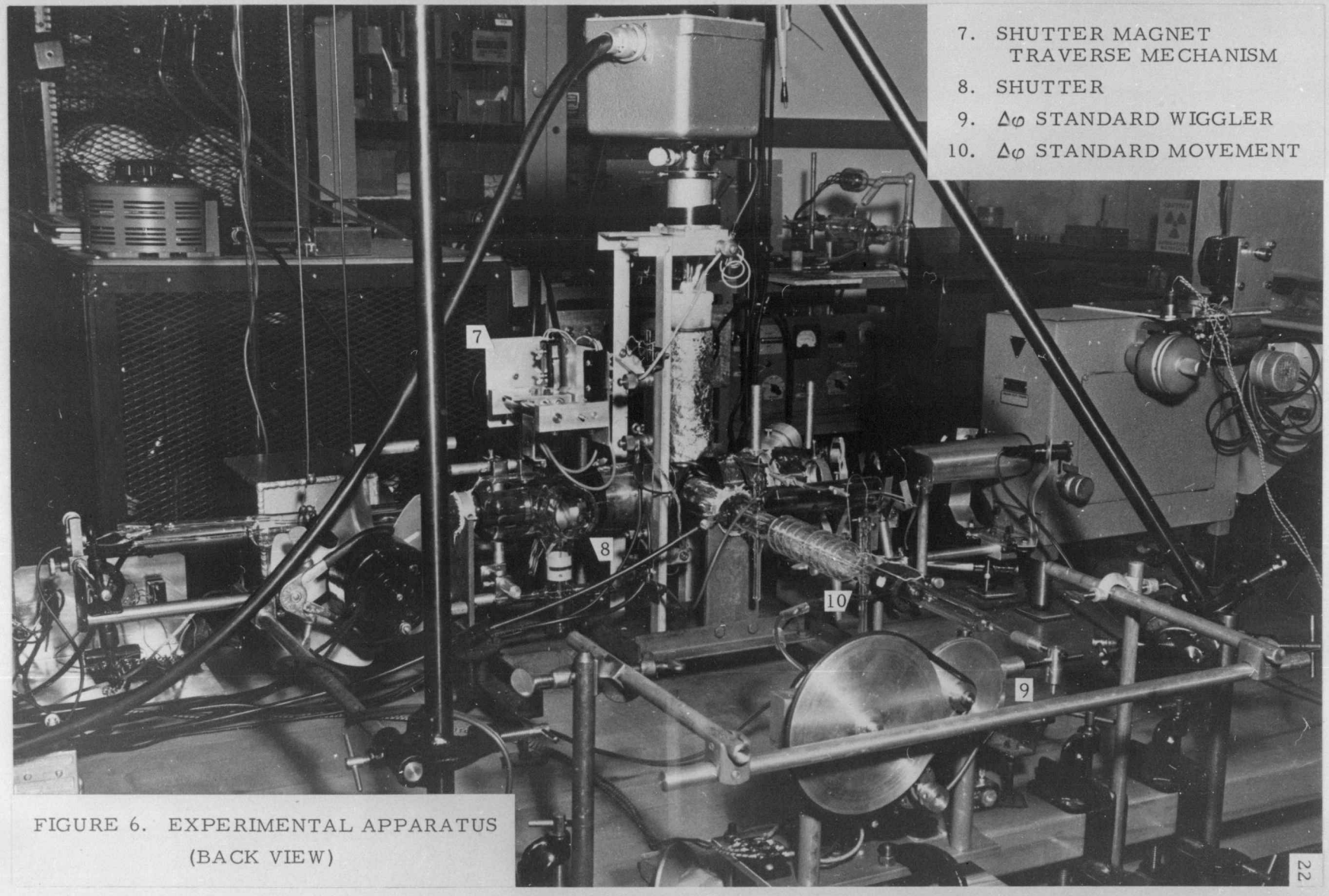

7. SHUTTER MAGNET TRAVERSE MECHANISM
8. SHUTTER
9. $\Delta\varphi$ STANDARD WIGGLER
10. $\Delta\varphi$ STANDARD MOVEMENT

FIGURE 6. EXPERIMENTAL APPARATUS (BACK VIEW)

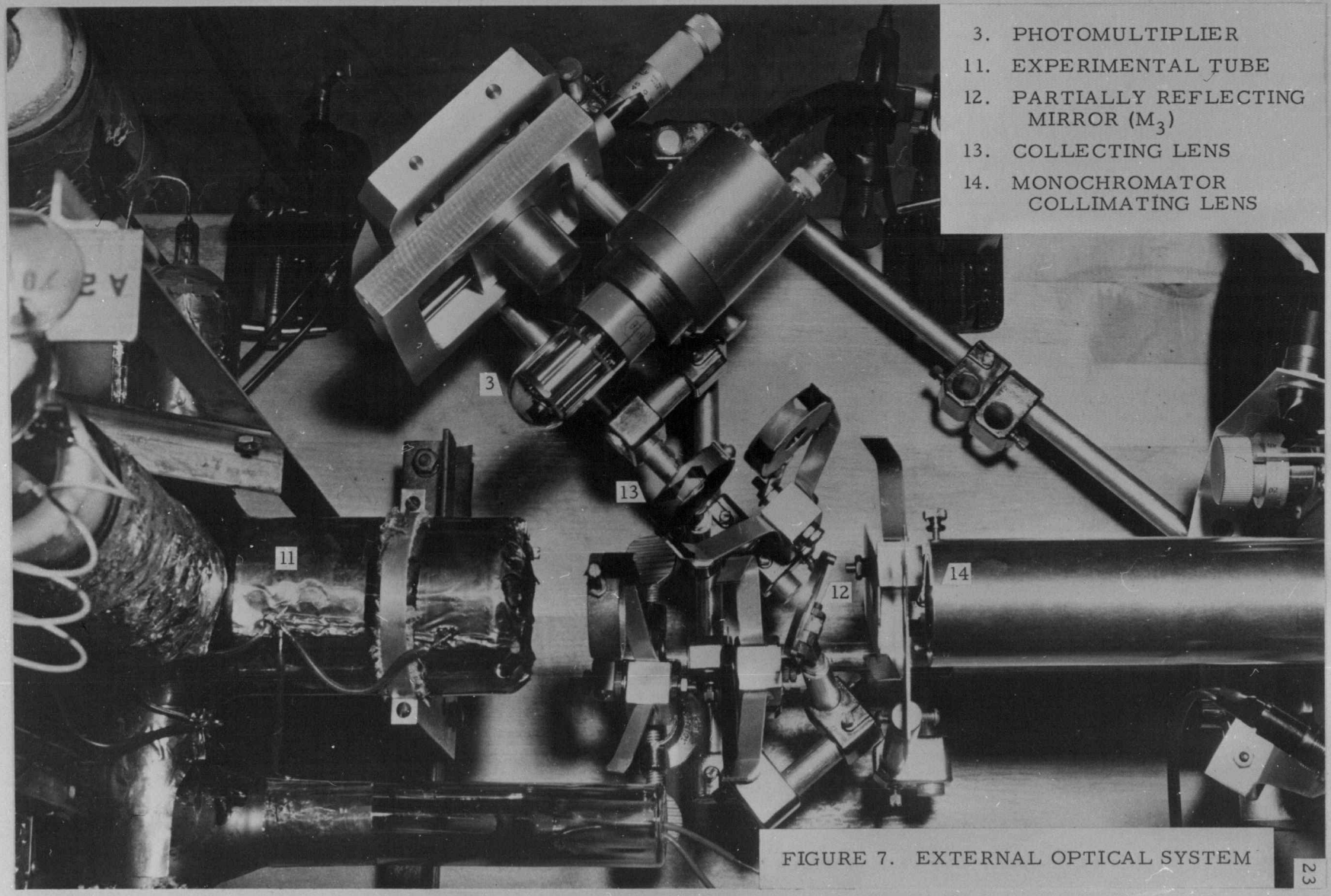

3. PHOTOMULTIPLIER
11. EXPERIMENTAL TUBE
12. PARTIALLY REFLECTING MIRROR (M_3)
13. COLLECTING LENS
14. MONOCHROMATOR COLLIMATING LENS

FIGURE 7. EXTERNAL OPTICAL SYSTEM

It was decided to use an arrangement by which a light beam would pass through the film twice by entering and being reflected out of the vacuum envelope along the same path. Since the output then depends on the square of the transmission the thickness measurement is more sensitive for the low absorption characteristic of the thickness interval with the most interesting properties. The optical system is shown schematically in Figure 8.

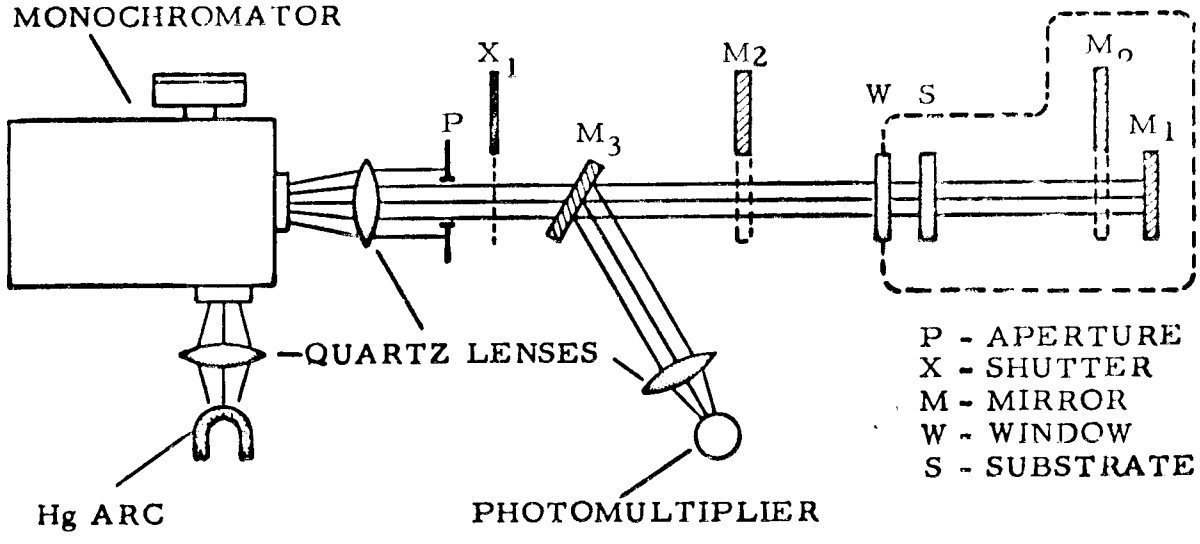

FIGURE 8. EXPERIMENTAL TUBE OPTICAL SYSTEM

As an introduction to optical system theory we will write first order approximations for the important quantities. We let t_n and r_n symbolize the transmission and reflection coefficients of a surface and I, the light intensity (which will generally expressed in terms of photomultiplier current).

In order to measure the light intensity incident on the tube, I_o, mirror M_2 is put in place. The background current, I_b, due to dark current and stray light is read with shutter X in place and is of course subtracted from all other readings. We can immediately write:

$$I = I_o r_2 r_3 + I_b \tag{18}$$

When M_o and M_2 are removed as is the case during photocurrent measurement, the photomultiplier output, I_B, is a monitor of the film illumination. Including first order terms only we can approximate the light intensity on the film, I_f, by the following equation:

$$I_f = t_w t_s I_o$$

In this case the monitoring detector will see a signal given by:

$$I_B = (t_w^2 t_s^2 r_f + I_B')I_o r_3 \tag{19}$$

which should be constant for each particular film thickness provided the source is of constant intensity. Here the small amount of light reflected from the window and substrate is symbolized by I_B'. Equation (19) gives the necessary information to normalize the photocurrent should the input light intensity vary during a photoemission run.

The measurement of film transmission is accomplished by utilizing two conditions--that with M_o in place and that with M_o removed from the

light beam. The expression for the signal, I_A, with M_o in place is:

$$I_A = r_3 I_o r_{system} + I_b$$

or:

$$I_A = r_3 I_o (2r_w + 2r_w^2 + t_w^2 t_s^2 r_f + t_w^2 t_s^2 t_f^2 r_o) + I_b$$

With M_o removed the r_o in the final term is replaced by r, the reflection coefficient of the end of the tube, and the signal is called I_B. Then subtraction of the two signals gives:

$$I_A - I_B = r_3 I_o (r_o - r_1) t_w^2 t_s^2 t_f^2$$

$$I_A - I_B = C\, I_o t_f^2$$

Since C_1 can be determined from initial conditions t_f may be obtained in this approximation. Note that r_f does not appear in this expression but both it and the absorption coefficient can be determined from I_B.

This rather simple idea serves as a basis for an exact expression involving infinite multiple reflections within the system.

At this point it is desirable to make firm definitions of the optical terms involved. Considering the antimony film a surface of negligible thickness (interference effects can be neglected) we can write:

$$I_{total} = I_{trans.} + I_{ref.} + I_{abs.}$$

or:

$$1 = t + r + a \qquad (20)$$

Note that according to Equation (20) the absorptance of a highly reflective surface will always be small since we are interested in the light absorbed in comparison with incident light. This definition seems most applicable for generalization to systems of surfaces.

Now consider a quartz flat of internal transmittance, t_q, as shown in Figure 9.

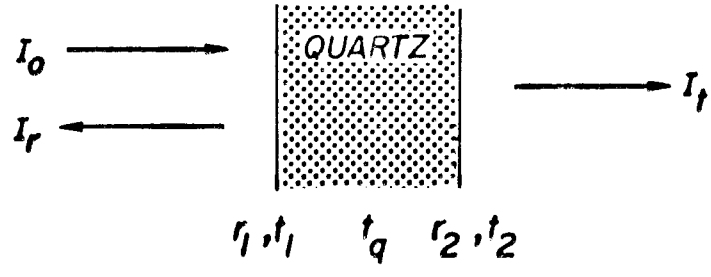

FIGURE 9. QUARTZ FLAT SCHEMATIC

Then the transmitted light, I_t, is given by:

$$I_t = I_o t_1 t_2 t_q + I_o r_1 r_2 t_1 t_2 t_q + I_o r_1^2 r_2^2 t_1 t_2 t_q + \cdots$$

Now if we sum this geometrical series we can write the composite transmittance, for the system, T_2, and similarly the reflectance, R_2:

$$T_2 = \frac{t_1 t_2 t_q}{1 - r_1 r_2 t_q^2} \tag{21}$$

$$R_2 = \frac{r_2 t_1^2 t_q^2}{1 - r_1 r_2 t_q^2} + r_1 \tag{22}$$

If $t_q = 1$, $t_1 = t_2 = 1 - r$, and $r_1 = r_2 = r$ for the quartz flat these equations simplify to:

$$T_2 = \frac{1 - r}{1 + r}$$

$$R_2 = \frac{2r}{1 + r}$$

We may proceed in this manner to find such coefficients for systems of surfaces but, in general (when $a \neq o$, $t_q \neq 1$) the equations are quite cumbersome and approximations are necessary. The problem could perhaps be handled more elegantly by transmission-reflection matrix for each surface but simplifications are easier in this straightforward method.

Since we will be making at least one approximation at the outset it may be well to tabulate the optical constants involved (Table 1). For the thickness determination a wave length of 4358 Å was used while photoemission was measured at 2482 Å, both of which are strong, clear lines from a mercury arc source.

TABLE 1. OPTICAL CONSTANTS OF FUSED QUARTZ

	λ,Å	n	r	t_q'
λ_p	2482	1.5077	0.04097	0.959
λ_t	4358	1.4677	0.03591	0.9934

n = Index of refraction

t_q' = Internal transmittance[4]

4. Values given are for a 1/16 inch thick, type 101 quartz disc and are taken from the General Electric Fused Quartz Catalog, Q7A.

The method of approach for a system of surfaces consists of writing a set of general equations for two surfaces and then considering the set as one surface having the derived coefficients. This can be extended to three surfaces by reapplication of the basic formula. Since internal transmission is quite different for the two wavelengths we are allowed different approximations and hence will separate the derivations into two different problems identified by the symbols λ_t and λ_p.

DERIVATION OF λ_t EQUATIONS In order to show in an intuitive way that we may neglect the absorption of quartz for λ_t let us consider the exact expressions for transmission and reflection of two surfaces. Our approximation to Equation (22) is:

$$R_2 = r_1 + \frac{t_1^2 r_2}{1 - r_1 r_2} \tag{23}$$

The error is using this approximation is given by:

$$\frac{\Delta R_2}{R_2} = \frac{\dfrac{1}{1 - r_1 r_2} - \dfrac{t_q^2}{1 - r_1 r_2 t_q^2}}{\dfrac{1}{1 - t_q^2 r_1 r_2}}$$

Since the maximum value of $r_1 r_2 \approx 1 - t_q^2 = 0.0032$

$$\frac{\Delta R_2}{R_2} \approx 1 - t_q^2 = 0.0032$$

By similar reasoning:

$$\frac{\Delta T_2}{T_2} \doteq 0.0016$$

It can be seen that the denominators of the exact equations (21) and (22) which express the effect of infinite multiple reflections are affected almost infinitesimally by the value of t_q. It is then reasonable to expect that since the bulk of the light output from the tube makes four transits of quartz discs the error can be approximated by:

$$\frac{\Delta R}{R}_{\text{tube}} \doteq (1 - t_q^4) = 0.0064$$

We will then use the following relations for the cases shown in Figure 10.

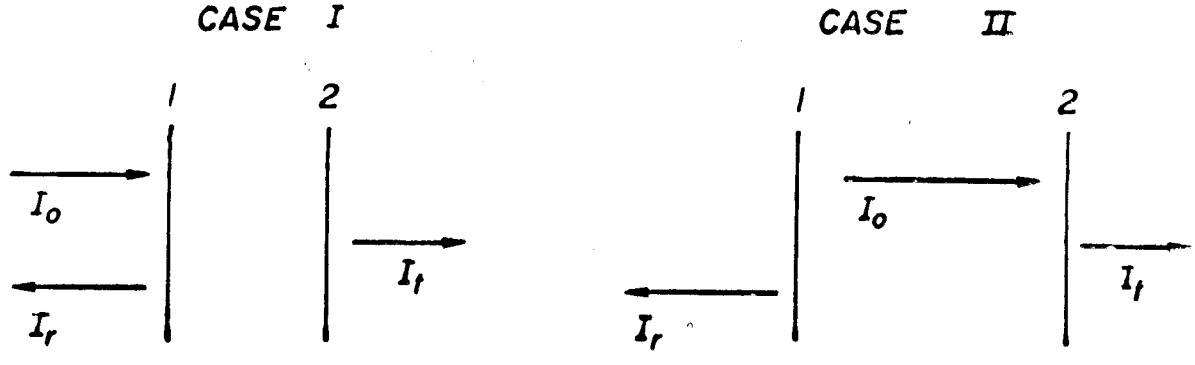

FIGURE 10. SURFACE CONFIGURATIONS

For Case I:

$$R_2 = r_1 + \frac{t_1^2 r_2}{1 - r_1 r_2}$$

$$T_2 = \frac{t_1 t_2}{1 - r_1 r_2}$$

For Case II:

$$R_2' = \frac{r_2 t_2}{1 - r_1 r_2}$$

$$T_2' = \frac{t_2}{1 - r_1 r_2}$$

By following the light path through the complete system (shown again schematically in Figure 11) we can write the final composite reflection of the system, R_A, by inspection. We have let $r_{1,2,3} = r_{quartz} = r$ and $t_{1,2,3} = (1 - r)$.

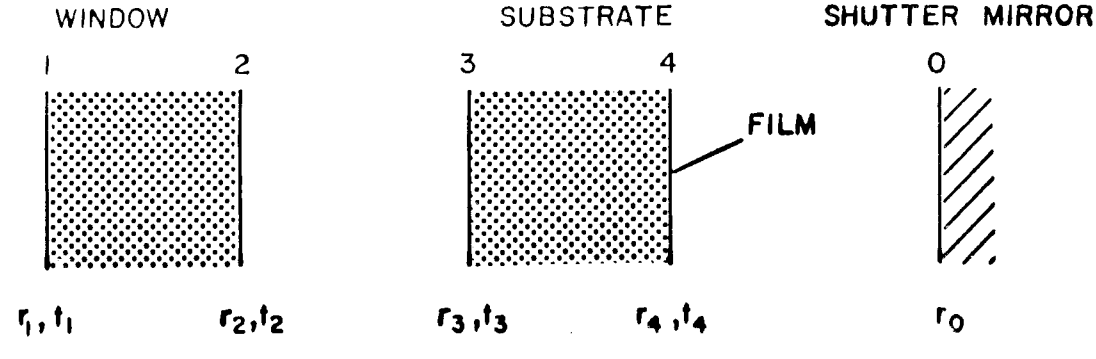

FIGURE 11. TUBE OPTICAL SYSTEM SCHEMATIC

$$R_A = r + (1-r)\left\{ \frac{r}{1+r} + \frac{1}{1+r}\left\{ \frac{r}{1+2r} + \frac{1+r}{1+2r}\left\{ \frac{(1-r)r_f}{(1+2r-3rr_f)} \right.\right.\right.$$

$$\left.\left.\left. + \frac{(1+2r)t_f}{(1+2r-3rr_f)}\left\{ \frac{r_o(1-r)t_f}{1+2r-3rr_f - r_o r_f(1+2r) + 3rr_o(r_f^2 - t_f^2)} \right\}\right\}\right\}$$

On combining terms we have:

$$R_A = \gamma + \frac{\delta r_f}{1-\gamma r_f} + \frac{\delta t_f^2 r_o}{(1-\gamma r_f)[(1-\gamma r_f) + \gamma r_o(r_f^2 - t_f^2) - r_o r_f]} \qquad (24)$$

where for convenience we have written:

$$\gamma = \frac{3r}{1+2r} = 0.100$$

$$\delta = \frac{(1-r)^2}{(1-2r)^2} = 0.808$$

for λ_t

Now if we move the shutter (M_o) out of the light path we replace r_o everywhere with r_1 in equation (24) and call the composite coefficient obtained R_B.

If ideal conditions prevailed it would now be a simple matter to find the desired quantities from the measurable quantitites.

$$I_A = r_3 I_o R_A + I_b$$

$$I_B = r_3 I_o R_B + I_b \qquad (25)$$

In determining the reflection coefficients for single mirrors considerable difficulty was experienced (and a great deepening of appreciation for "ideal conditions"). It is obvious that if the light beam is spatially uniform placement of an aperture before the photomultiplier will allow a certain amount of latitude in beam position without change in measured intensity. This is true no matter how non-uniform the sensitivity of the detector is. With the long optical levers in the system such latitude in alignment is almost a necessity.

Although the beam from the monochromator could be collimated satisfactorily, its projection was quite non-uniform at all usable slit settings. After refining the experimental system as much as possible it was finally necessary to define a collection coefficient, K, for each function of the system which expressed the relative amount of light finding its way to the detector. Thus we must rewrite Equation (25):

$$\begin{aligned} I_A &= r_3 K_A I_o R_A \\ I_B &= r_3 K_B I_o R_B \\ I_1 &= r_3 r_2 K_o I_o \end{aligned} \tag{26}$$

Dividing by Equation (26) and substituting a new set of coefficients we have:

$$\begin{aligned} A &= \frac{I_A}{I_1} = \frac{K_A R_A}{r_2 K_o} = \alpha R_A \\ B &= \frac{I_B}{I_1} = \frac{K_B R_A}{r_2 K_o} = \beta R_B \end{aligned} \tag{27}$$

OPTICAL SYSTEM CALIBRATION By using the theoretical reflectance of the quartz flats we can, by blocking various portions of the optical system, calculate the constants α, β, r_0, r_1, and r_2. The optical system was set up as in Figure 12. (For the shutters X_2 and X_3, $r = t = 0$.)

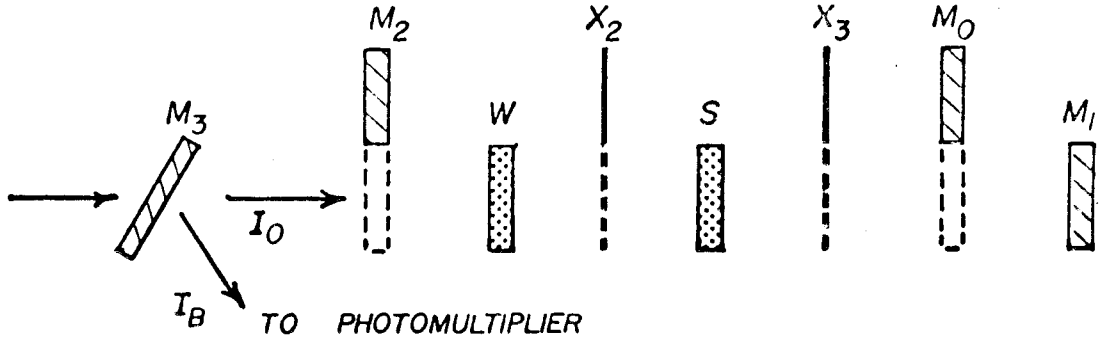

FIGURE 12. OPTICAL SYSTEM DURING INITIAL CALIBRATION

We can immediately write the following expressions using Equations (24 and (27):

1. With shutter X_3 in place (before film deposition--hence $r = r_f$) we have:

$$B_1 = \beta \left\{ \gamma + \frac{r_f}{1 - \gamma r_f} \right\} \tag{28}$$

From this we can calculate $\beta = 1.96$ using experimental values.

2. With shutter X_2 in place we can write:

$$B = \beta' \left\{ \frac{2r}{1 + r} \right\}$$

Experiment shows $\beta' = 1.95$ using measured values. Since Equation (28) is supported by better data we will use $\beta = 1.96$. If it is now assumed that K_o and K_β are close to unity then $r_2 = 0.51$.

3. With only the tube reflection, r_1, in effect the equation is:

$$B_3 = \beta\left\{\gamma + \frac{\delta r}{1-\gamma r} + \frac{r_1(1-r)^2}{(1+3r)[1+er-4rr_1]}\right\}$$

and we find $r_1 = 0.0031$.

4. With M_o in place we have:

$A = \alpha R_A$ and since $r_f = r$ and

$t_f = (1-r)$ this reduces to:

$$A = \alpha\left\{\gamma + \frac{\delta r}{1-\gamma r} + \frac{r_o(1-r)^2}{(1+3r)(1+3r-4rr_o)}\right\} \qquad (29)$$

Now if we set $\alpha = \beta$ we find $r_o = 0.635$, a value which is consistant with preliminary reflection measurements.

Since $dr_o \doteq 0.37\, d\alpha$ and α should be within a few percent of β the possible error in r_o is quite small. Note that we cannot find r_o and α independently with the calibration techniques used here. In effect we have calibrated the system at both maximum and minimum transmission (Equations (28) and (29)) so it is quite appropriate to set $\alpha = \beta$.

In order to permit quick evaluation of film thickness during the progress of the experiment we wish to simplify the computations leading to t_f and r_f as much as possible. The output data is A and B as defined by Equation (27) and we form the difference after introducing the following variables:

$$x = \delta t_f^2, \quad y = 1 - \gamma r_f, \quad z = \gamma(r_f^2 - t_f^2) - r_f$$

$$A \cdot B = \frac{\beta x}{y^2(1 - z r_o/y)} \left\{ r_o - \frac{r_1(1 + z r_o/y)}{1 + z r_o/y} \right\}$$

Since $-0.3 > \frac{z}{y} r_o > 0$ the factor of r_1 is less than unity and the maximum error in neglecting the last term in the brackets is:

$$\frac{r_1}{r_o} = \frac{0.003}{0.635} = 0.0047$$

Over most of the range of film thickness $\frac{z r_o}{y} \doteq -0.1$ so if we simply use $(r_o - r_1)$ in place of r_o the error is reduced to about 0.1%.

Our difference expression is now:

$$\frac{A-B}{\beta\delta(r_o - r_1)} = \frac{t_f^2}{(1-\gamma r_f)[(1-\gamma r_f) + \gamma r_o(r_f^2 - t_f^2) - r_o r_f]}$$

Expanding the left side of this equation we have the terms listed in Table 2. In this table we have used film number as a convenient parameter expressing film thickness. Forty-one thickness increments were used in building up a film approximately 300 Å thick. The important variations are slow enough so that five term maximums are adequate for error analysis.

TABLE 2. MAXIMUM TERM VALUES FOR EQUATION (30)

Film Number	0	10	20	30	40
r_f	0.04	0.02	0.03	0.18	0.50
t_f	0.96	0.81	0.63	0.22	0
Numerator term					
t_f^2	0.92	0.66	0.63	0.22	0
Denominator terms					
1	1	1	1	1	1
$-2\gamma r_f$	0.008	0.004	0.006	0.036	0.10
$+2\gamma r_o r_f^2$	0.0002	0.00005	0.00011	0.0041	0.032
$-\gamma r_o t_f^2$	0.058	0.042	0.025	0.0032	0
$-r_o r_f$	0.025	0.012	0.019	0.11	0.32
$+\gamma^2 r_o r_f t_f^2$	0.00023	0.00008	0.00008	0.00005	0
$+\gamma^2 r_f^2$	$\sim 10^{-5}$	$\sim 10^{-5}$	$\sim 10^{-5}$	0.0032	0.0025
$-\gamma^2 r_o r_f^3$	$\sim 10^{-6}$	$\sim 10^{-6}$	$\sim 10^{-6}$	0.00004	0.0008

Since the last three terms may be neglected with $< 0.3\%$ error in the denominator, we are left with:

$$C = \frac{A-B}{\beta\delta(r_o - r_1)} = \frac{t_f^2}{1-(2\gamma+r_o)r_f + 2\gamma r_o r_f^2 - \gamma r_o t_f^2} \tag{31}$$

Rearranging we have:

$$f(r_f) = 1-(2\gamma + r_o)r_f + (2\gamma r_o)r_f^2 = t_f^2\left\{\frac{1}{C} + \gamma r_o\right\}$$

Then solving for t_f^2 we can write:

$$t_f^2 = f(r_f)\left\{\frac{C}{1+C\gamma r_o}\right\} = r(r_f)\ g(C) \tag{32}$$

It remains to show the procedure for determination of r_f from B.

$$B = \beta\left\{\gamma + \frac{\delta r_f}{1-r_f} + \frac{t_f^2 r_1}{(1-\gamma r_f)[(1-\gamma r_f)+ \gamma r_1(r_f^2 - t_f^2)- r_1 r_f]}\right\}$$

When the denominator of the last term is expanded it is clear that we can neglect all terms except $1-2\gamma r_f$ and B is given to good accuracy by:

$$B = \beta\left\{\gamma + \frac{\delta r_f}{1-\gamma r_f} + \frac{\delta t_f^2 r_1}{1-2\gamma r_f}\right\} \qquad (33)$$

We must now show that the error involved in neglecting the last term involving t_f^2 is small. (An iterative scheme to calculate r_f exactly involving Eqautions (32) and (33) might have been used to advantage had experimental precision warranted it.)

Letting x symbolize the last term in Equation (33) we find the first derivative approximation for the change in r_f due to neglect of x:

$$\frac{dr_f}{dx} = \frac{(1-\gamma r_f)^2}{\delta} \quad .$$

Since the maximum value of r_f is 0.02 the error in r_f is given approximately by $\Delta r_f = \frac{\Delta x}{\delta} = 0.0034$. Following this error through the expression for film transmission we find a change of around 0.1% .

Finally Equation (33) can be written:

$$r_f = \frac{B - \gamma\beta}{B\gamma + \delta\beta - \gamma^2\beta} \qquad (34)$$

The functions developed above (Equations (31), (32), and (34)) are plotted against the measurable quantitites, A and B, and the film transmission can be quickly computed.

In order to make use of the transmission data we must look at the methods used in Condas' experiment (6). His procedure was to compare the transmitted light through a blank substrate with that through a film coated substrate. Then his transmission coefficient, t_c, is given by:

$$t_c = \frac{t_f}{1 - r}$$

where r is the reflection coefficient of the quartz.

Condas' data was given for three wavelengths: 4500 Å, 5380 Å, and 6650 Å. Inspection of the mercury arc spectrum shows the 4358 Å line to be a logical choice because of its isolation, intensity, and proximity to the data curve of Condas'. Plots were made of t_c against λ and the value of t_c at λ_t = 4358 Å was obtained by extrapolation. The final plot of t_c against film thickness is shown in Figure 13. The anomalous behavior of the amorphous film (τ < 110 Å) is shown dramatically in a $\ell n\, t_c$ plot in the same figure. Following this are Figures 14 and 15 showing reduction of the data obtained. Discussion of the final conversion to film thickness will be appropriate in the

metal source section because of certain adjustments to be made there.

Because of the complicated nature of the system no strictly analytical error treatment was attempted. Instead it is appropriate to list the sources of error, using experience with the apparatus to fix their approximate magnitudes (see Table 3).

TABLE 3. ERROR ESTIMATE FOR OPTICAL SYSTEM (λ_t AND λ_p)

Error	Approximate Magnitude (Effect on t_f) λ_t	λ_p
Errors from theory		
Neglect of t_q	-0.3%	---
Indeterminacy of α	±0.8%	±1 %
Neglect of r_1 term	±0.2%	±0.2%
Neglect of denominator terms of A	+0.3%	+0.3
Neglect of t_f^2 term of B	-0.1%	-0.1%
Instrument Errors		
Photomultiplier nonlinearity and variation in sensitivity	<1 %	<1 %
Chart recorder	±0.5%	±0.5%
Light intensity variation	Compensated	
Fundamental system errors		
Lack of reproducibility due to M_o	±1 %	±2 %
Light scattering error (estimated)	~3 %	~3 %
Variable absorption in UV due to surface films on quartz flats and mirrors	---	<4 %

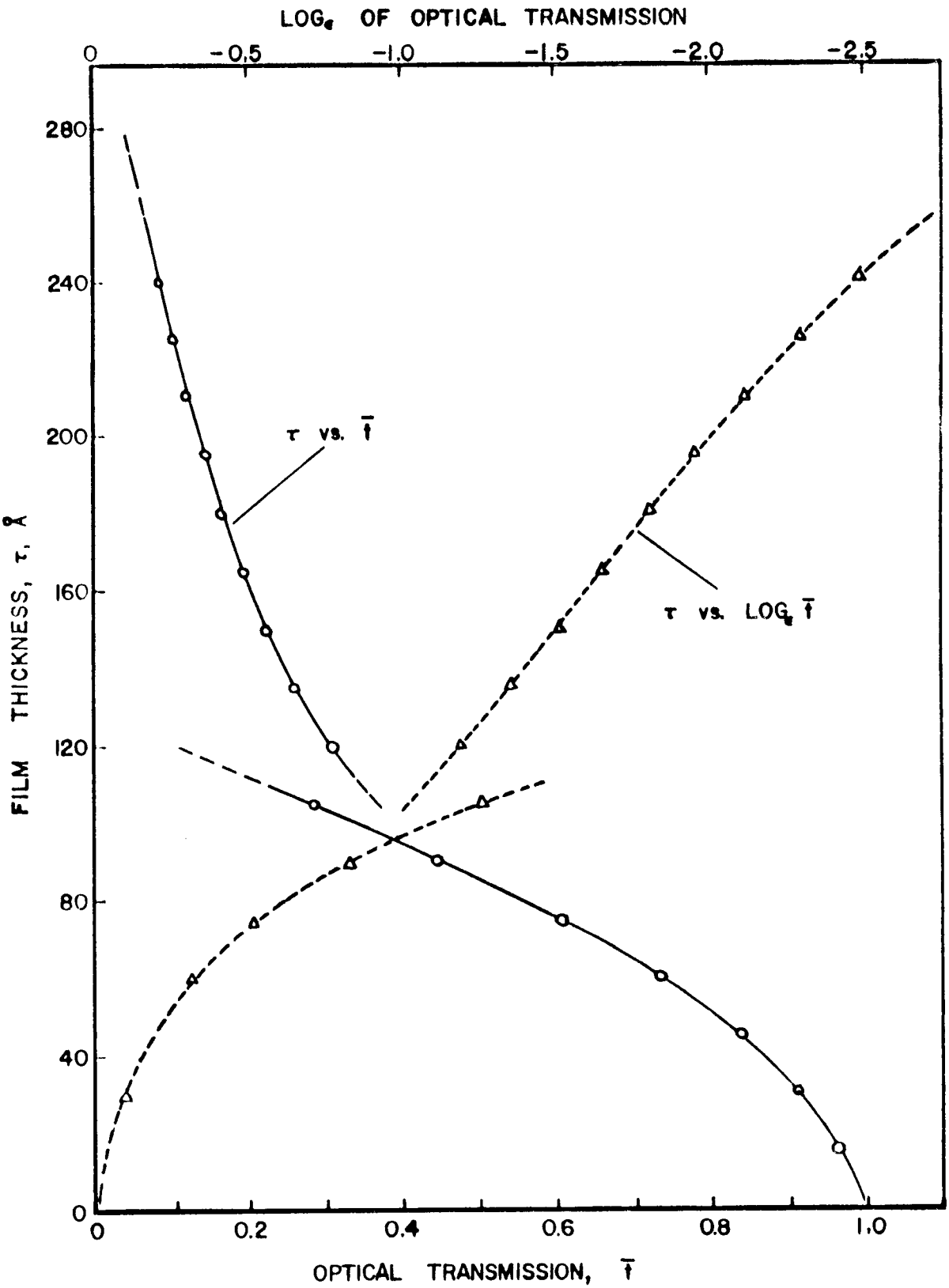

FIGURE 13. OPTICAL TRANSMISSION VERSUS FILM THICKNESS FOR ANTIMONY AT λ = 4358 Å

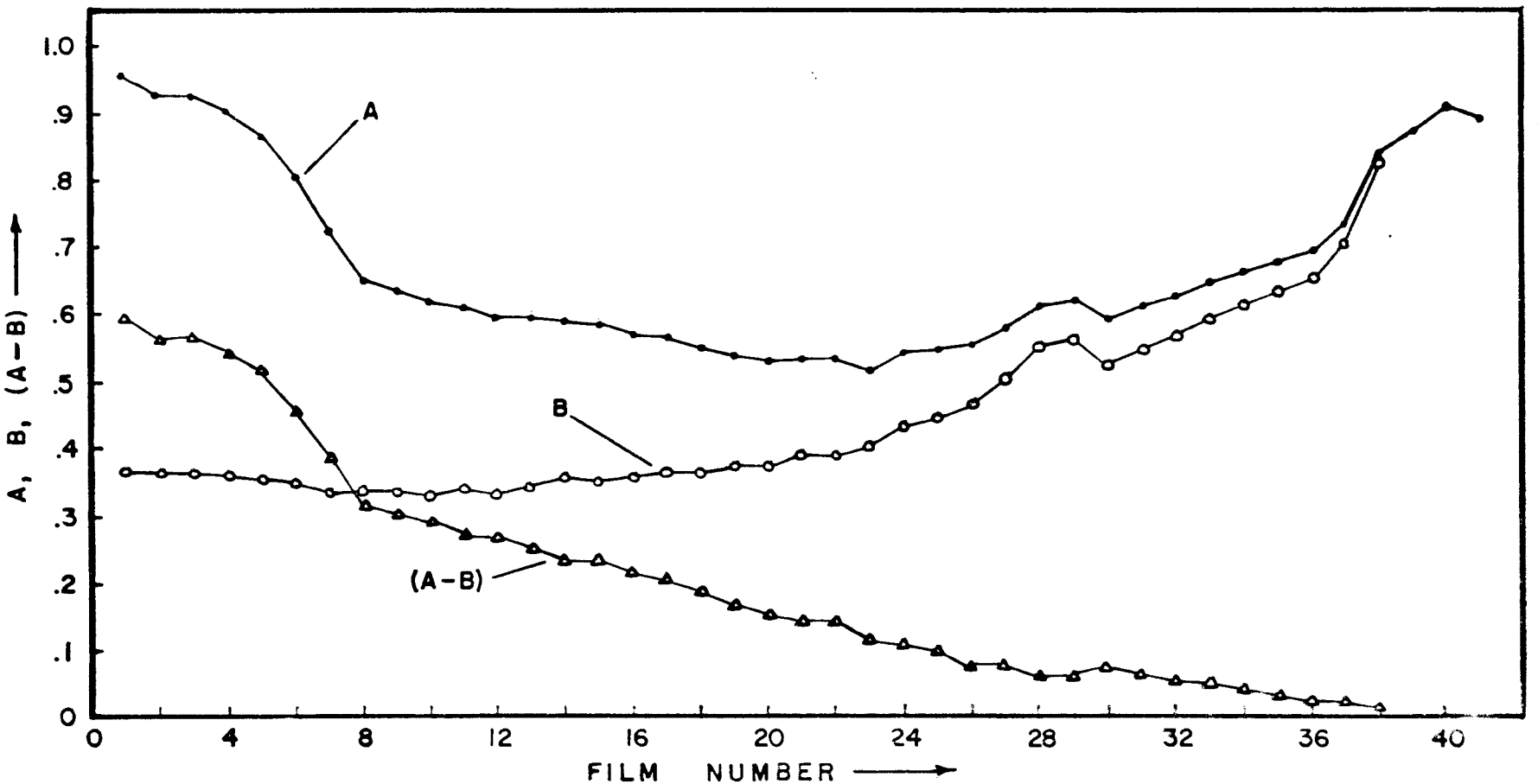

FIGURE 14. λ_p OPTICAL PARAMETERS (FOR OPTICAL PROPERTIES)

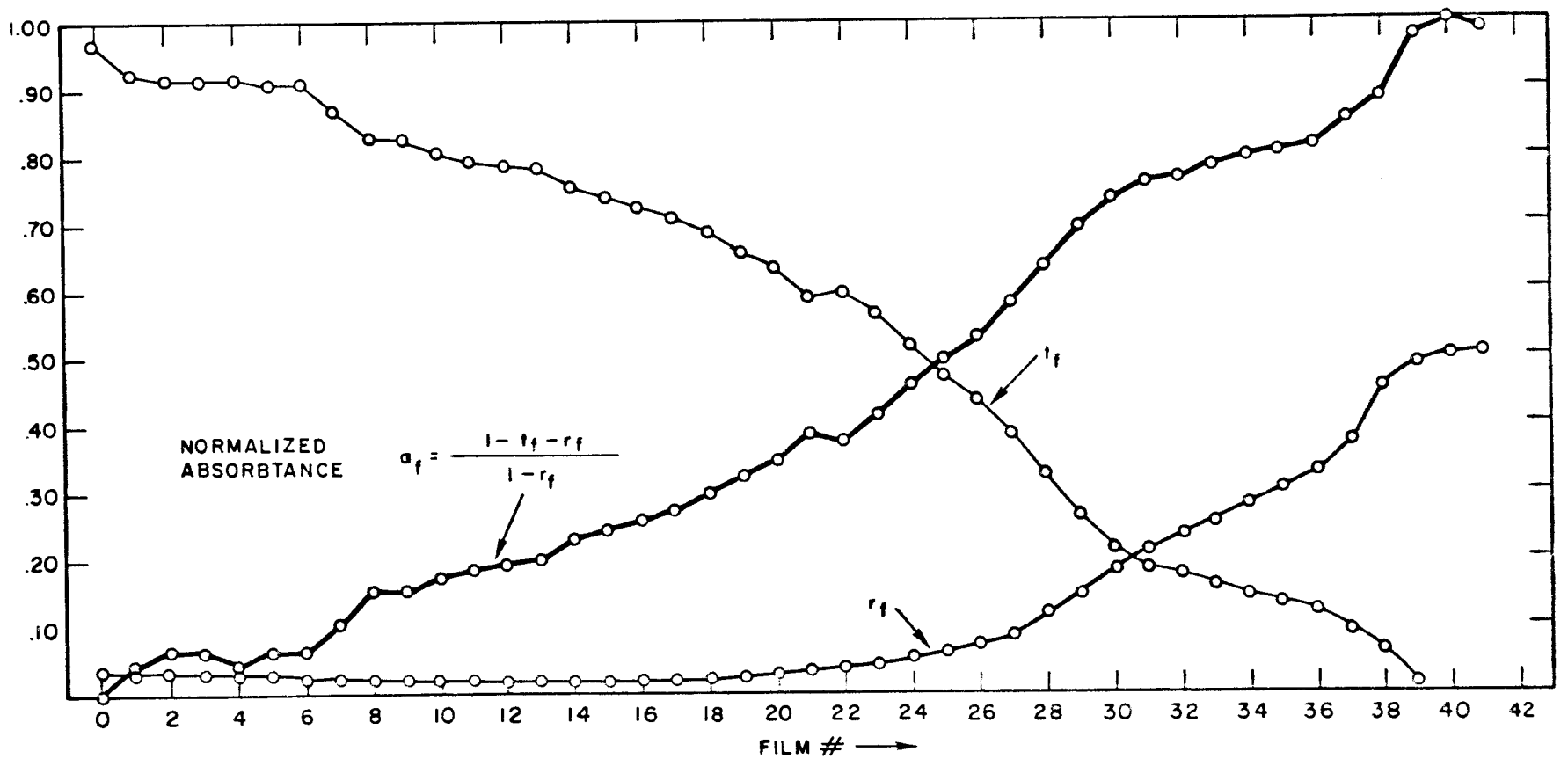

FIGURE 15. λ_t OPTICAL COEFFICIENTS

DERIVATION OF λ_p EQUATIONS The measurement of optical coefficients at the photoemission wavelength is necessary to establish how much light was absorbed in the film. Except for some complications introduced by the absorption of the quartz flats, the derivations and error treatment for the photoemission wavelength follow the same general plan as those for λ_t above. Using the equations for the composite coefficients for two surfaces (Equations (21), (22)) as a starting point it is clear that the most inclusive reflection and transmission coefficients which do not depend on variable parameters are those for the first three surfaces, R_3, $\bar{R}_3$, and T_3, so the final expressions will be written in terms of these. Note that while R_2 is symmetrical with respect to direction of light travel R_3 is not and so the coefficient for left-ward traveling light is denoted $\bar{R}_3$ (see Figure 11).

These expressions are:

$$R_3 = \frac{r(1 + t_q^2 - 2rt_q^2)}{(1 - r^2t_q^2)} + \frac{(1 - r)^4 rt_q^2}{(1 - r^2t_q^2)(1 - 2r^2t_q^2 - r^2 + 2r^3t_q^2)}$$

$$\bar{R}_3 = \frac{r(2 - 2r + t_q^2 - 4rt_q^2 + 3r^2t_q^2)}{(1 - r^2 - 2r^2t_q^2 + 2r^3t_q^2)}$$

$$T_3 = \frac{(1 - r)^3 t_q}{(1 - r^2 - 2r^2t_q^2 + 2r^3t_q^2)}$$

On making the following substitutions the equation for R_A can be written in a familiar form:

$$\gamma = R_3 \qquad \delta = T_3^2 t_q^2 \qquad \bar{\gamma} = \bar{R}_3 t_q^2$$

$$R_A = \gamma + \frac{\delta r_f}{1 - \bar{\gamma} r_f} + \frac{\delta r_o t_f^2}{(1 - \bar{\gamma} r_f)[1 - \bar{\gamma} r_f - r_f r_o + \gamma t_q^2 r_o (r_f^2 - t_f^2)]} \tag{35}$$

On replacing r_o by r_1 this becomes the expression for R_B. At this point the expressions are exact.

A calibration procedure much like that for λ_t (see page 34 and Figure 12) gives $\beta = 2.69$ and $\beta' = 2.63$ for the two determinations of collection coefficient and is an indication of system consistancy. Finally $r_1 = 0.0024$ and setting $\alpha = \beta$ gives $r_o = 0.376$ for the shutter-mirror reflectance.

With the system parameters determined we are ready to simplify the equations for computation. Setting $\alpha = \beta$ as before we form the difference, $R_A - R_B$:

$$R_A - R_B = \frac{\beta \delta t_f^2}{1 - \bar{\delta} r_f} \left\{ \frac{r_o}{[1 - \bar{\gamma} r_f - r_f r_o + \gamma r_o t_q^2 (r_f^2 - t_f^2)} - \frac{r_1}{[1 - \bar{\gamma} r_f - r_f r_1 + \gamma r_1 t_q^2 (r_f^2 - t_f^2)]} \right\}$$

In order to neglect the last term above we note that its maximum value is approximately 0.008 and if we simply change r_o from 0.376 to 0.375 in the first term only a small loss in accuracy ($< 0.1\%$) will result from the simplification.

Using λ_t type developments we can again equate t_f^2 to a product of single variable functions making rapid analysis possible. The error estimate is shown in Table 3.

The plot of optical parameters versus film number (Figure 16) shows less quality than that for λ_t principally because of the variation of the reflectance of M_o over its surface.

FILM ILLUMINATION In order to determine the amount of light incident on the film, I_f, let us first consider an approximation made earlier in terms of incident intensity:

$$I_f \approx t_w t_s I_o$$

This quantity is perturbed slightly by the changing reflectance of the film iteslf since a portion of the light undergoing multiple reflections is re-incident on the film.

During photoemission, the optical system is as shown in Figure 17. The major difference between this and the system during measurement of optical parameters is the beam size; an aperture, P_o, (1/2 inch diameter) is replaced by P_1 which limits the incident beam to a diameter of 1-1/8 inches. In order to reduce the sensitivity of the detector system a 1/2 inch aperture, P_2, and an absorber (a quartz flat with ground finish on one side), A_1, is placed immediately before the collecting lens for the photomultiplier.

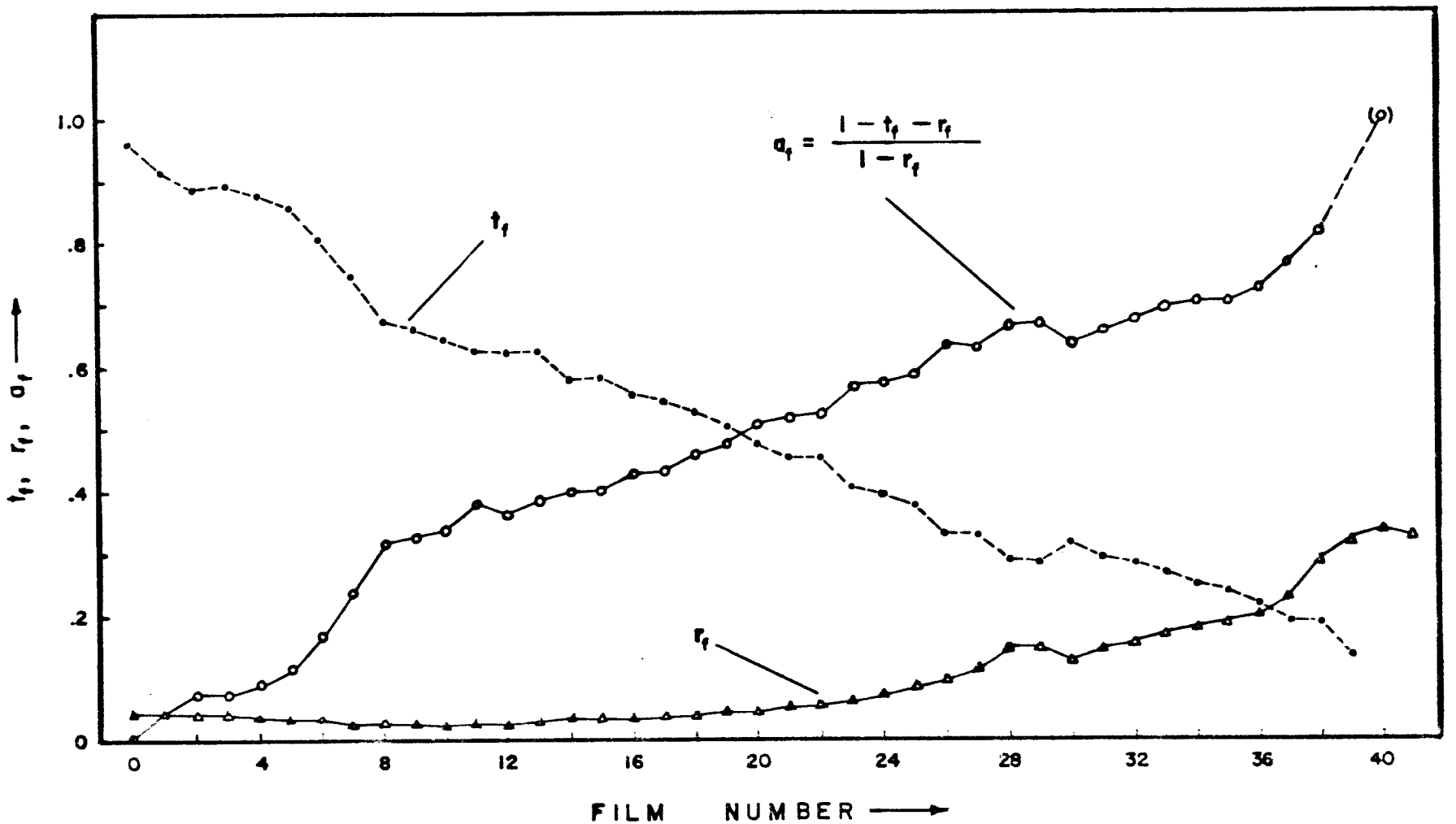

FIGURE 16. FILM TRANSMISSION, REFLECTION, AND ABSORPTION COEFFICIENTS FOR λ_p

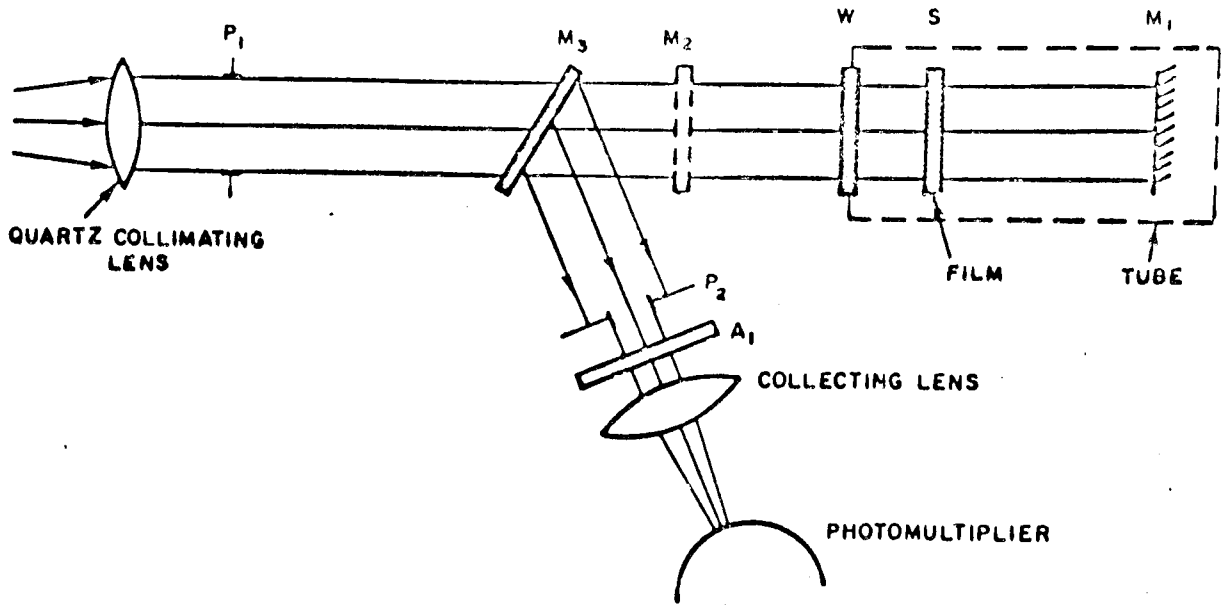

FIGURE 17. PHOTOEMISSION OPTICAL SYSTEM

Since intensity is standardized by placement of M_2 in the beam, giving a signal I_{1f},[5] the film illumination is dependent on the constancy of photomultiplier sensitivity. We expect this to remain constant enough for the purposes of this experiment in view of stability tests run previously.

During photoemission we are monitoring the value of I_f (indirectly by observation of I_{Bf}) in order to apply corrections to the photocurrent which is simultaneously being recorded. An approximation to this monitor signal is given below:

$$I_{Bf} = K_{Bf} r_3 I_o R_{Bf} \doteq K_{Bf} r_3 I_o (t_w^2 t_s^2 r_f + I_B')$$

where I_B' includes window reflections, etc.

---

5. We will subscript quantities pertaining to film illumination measurements with an f.

Ideally we would expect the detector system collection coefficients, K_o and K_B, defined earlier, to be of nearly the same values as those measured and the solution for I_f to follow directly by the use of the measured value of r_f. On computing $B_f = I_{Bf}/I_{1f}$ for this function of the system however it was found to be considerably different than the B computed during the λ_t transmittance run (see Figure 18). Comparison of data taken with both beam sizes shows a small difference in the ratios of A to B and A_f to B_f ($\sim$ 3%) but a large change in the value of $B(B_f \doteq 2B)$; therefore we can attribute most of the change to the value of the collection coefficient,[6] K_o, or more generally $K_o r_3 r_2$. However the consistant disagreement in the interval between films 2 and 20 must be due to an r_f dependent effect which in turn must occur either within the function $R_{Bf}(r_f)$ or be the result of scattering which is dependent on film thickness.

We are interested in an order-of-magnitude approximation for I_f based on photomultiplier sensitivity and an accurate ratio by which to normalize photocurrent for changes in I_f. Because the photocurrent correction is small it is given to sufficient accuracy by a function of r_f as measured previously. The reference intensity is given by:

$$I_f = \xi K_{of} r_2 r_3 I_o = C_o I_o \qquad (36)$$

where ξ is the coefficient of the attenuators A_1 and P_2. By methods outlined before it is a simple matter to calculate the infinite

---

6 K_o is the collection coefficient for the standardizing mirror function (M_3 in position).

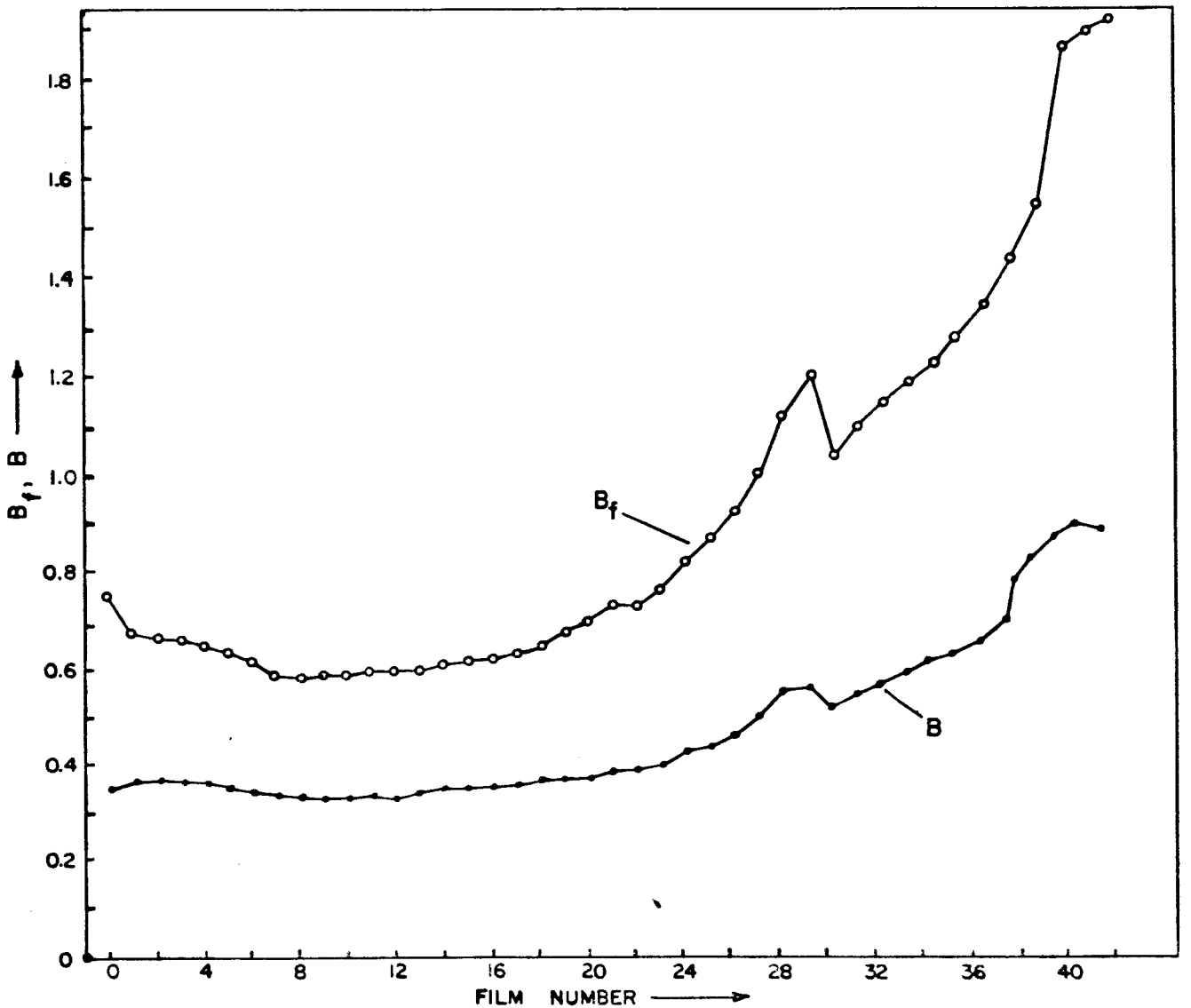

FIGURE 18. λ_p OPTICAL PARAMETERS (FOR FILM ILLUMINATION)

re-reflection expression for I_f:

$$I_f = \frac{I_o t_q T_3}{1 - t_q r_f R_3} = \frac{I_o \sqrt{\delta}}{1 - \bar{\gamma} r_f}$$

Then using Equation (36) we have:

$$I_f = \frac{\sqrt{\delta}\, I_{1f}}{\gamma C_o (1/\bar{\gamma} - r_f)} = \frac{420\, I_{1f}}{(9.8 - r_f)}$$

using experimental values for evaluation. In terms of recorder output this is:

$$I_f, \ \mu \text{watts/cm}^2 \approx 2.6 \times 10^{-5} (I_{1f}, \text{mv})$$

which means the approximate film illumination was 2.3×10^{-4} μ watts/cm^2.

The correction to be applied to I_f consists of adjustment to the reference level and use of the factor shown below:

$$0.998 < \frac{9.76}{9.8 - r_f} < 1.04$$

where the denominator is chosen to make the factor unity at the most common value of r_f.

EXPERIMENTAL PROBLEMS Thus far we have only casually mentioned experimental (or technical) aspects of the optical system. Now in order are some comments about the special problems involved with the stability and spatial uniformity of the light source and detector and the reliability of the mirror system.

The time stability of both the light source and detector were investigated in order to determine the feasibility of comparison of intensities with a single detector. The test set-up shown in Figure 19 is essentially the same as that used during the experiment.

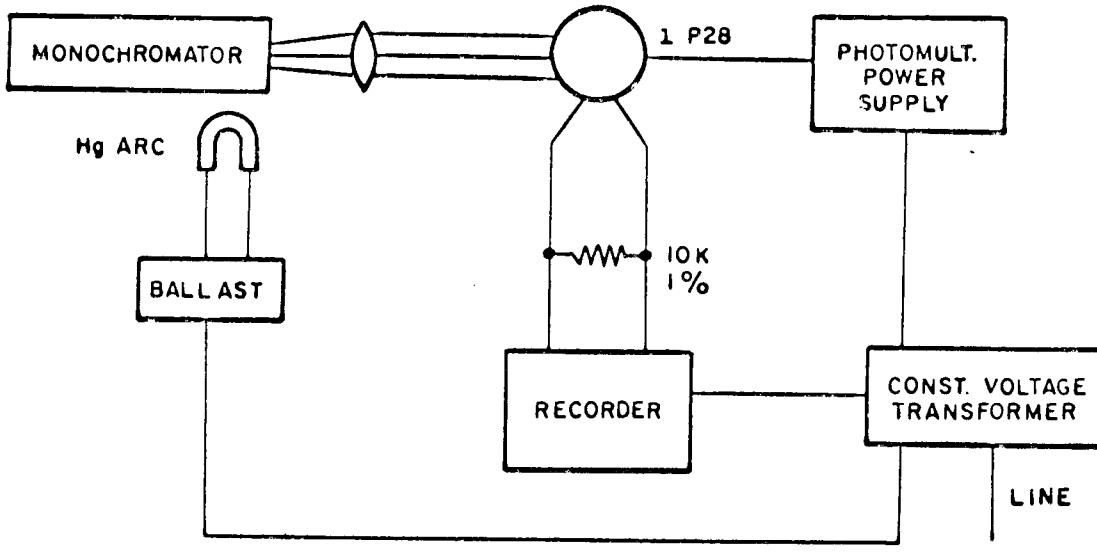

FIGURE 19. OPTICAL SYSTEM INSTRUMENTATION

After the mercury arc and detector power supply were warmed up ~ 10 hours a stability run was made using the 3640 Å mercury line. With the photomultiplier output at about 90 μamps it was found that the output decayed at a rate of 1/4% per minute. Noise of about 2% amplitude and random period and waveshape was also noticed (0.05 sec $\leq$ 10 sec). On switching the photomultiplier high voltage supply some recovery was noted for on and off periods as short as 20 seconds. Moderate vibration of system parts did not affect output appreciably.

A second test using a continuous, tungsten filament light source powered by two large, well-charged storage batteries showed that most of the noise was inherent in the mercury arc light source and that the decay observed was due to high photomultiplier current. A change to 10 μamp anode current resulted in a very uniform and stable trace for the tungsten source.

Adjustment of the Hg arc image on the monochromator input slit improved conditions and indicated that the source of part of the noise was due to actual movement of the arc within its envelope. With the system adjusted carefully the noise amplitude was about one percent and a capacitor of suitable time constant across the recorder terminals gave a stable trace.

Data for various signals (i.e., I_1, I_o, I_B) were taken by adjacent comparison which permitted accurate measurements despite changes in light intensity and detector sensitivity. Two intensities were compared from 5 to 15 times, each being recorded for ~ 10 seconds. A representative record is shown in Figure 20.

During construction of the apparatus it was rather naively assumed that the spatial uniformity of the light beam and detector system was well behaved enough to allow minor misalignments in the optical system. This proved to be one of the most exasperating difficulties of the experiment.

After many first-thought attempts of a quick solution of the problem an exhaustive investigation seemed the only answer. Removal of

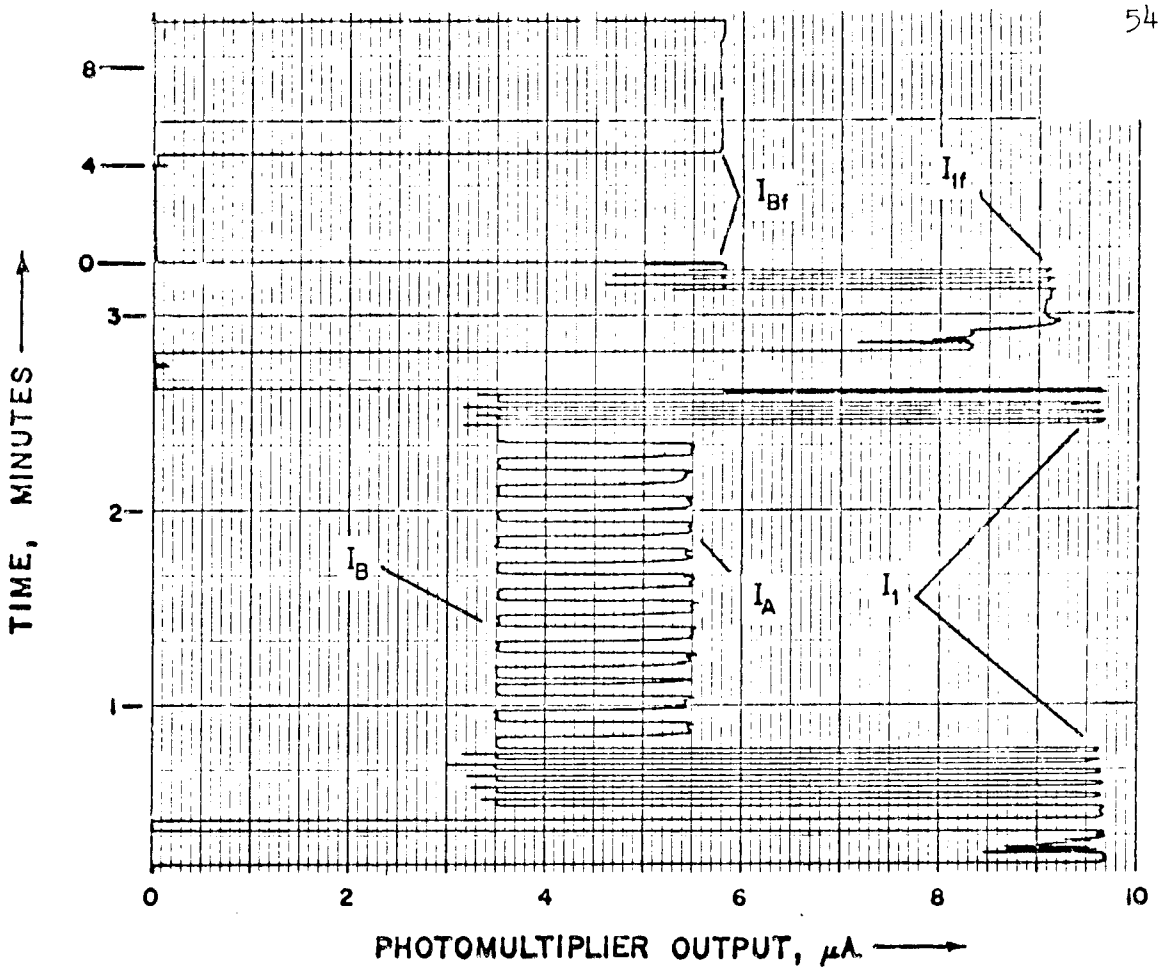

FIGURE 20. OPTICAL DATA CHART RECORD

the exit lens of the monochromator (which partially collimates the output) showed an easily visible star-shaped intensity pattern at all reasonable slit settings. A new, larger monochromator proved more non-uniform than the first. Removal of the exit lens allowed only the more uniform central portion of the pattern to fall on the final collimating lens and improved things somewhat giving a variation of something like 30% across the beam (sacrificing intensity in the process however). Placement of a diffuser at a focal point might have been a possible solution if the loss in intensity could have been tolerated.

The extreme non-uniformity of the photomultiplier effectively sampled the remaining variation in light intensity much like a pin hole swept across the beam. Most of the difficulty originated with the nonregistry of the reflection of M_o since the optical lever involved here was 53 cm. Due to the construction of the stops and pivot for the mirror it would not reproduce its position exactly and a misalignment of only five seconds of arc seriously affected the output signal.

When adjusting the photomultiplier to the position of maximum response proved inadequate a quartz collecting lens was used to focus the light into a small spot. However the grid wires before the photosensitive surface in the photomultiplier were now able to contribute to the trouble since the best spot size was now comparable to the grid spacing (0.5 mm). Despite this the collecting lens method gave better results. An end window photomultiplier would have solved the difficulty with the existing setup but the required ultra-violet sensitivity made such a tube prohibitively expensive.

In order to determine the spatial sensitivity of the 1P28 photomultiplier cathode and to make precise alignment possible the photomultiplier was scanned with a one millimeter beam on two axes with the results shown in Figure 21. To do this the phototube was mounted on two micrometer movements making precise axial and transverse positioning possible (X, along the cylindrical axis of the photomultiplier and Y transverse). These were driven by a slow synchronous motor while flashes of light on exact revolutions of the micrometer barrel provided reference marks for the chart record. The mounting

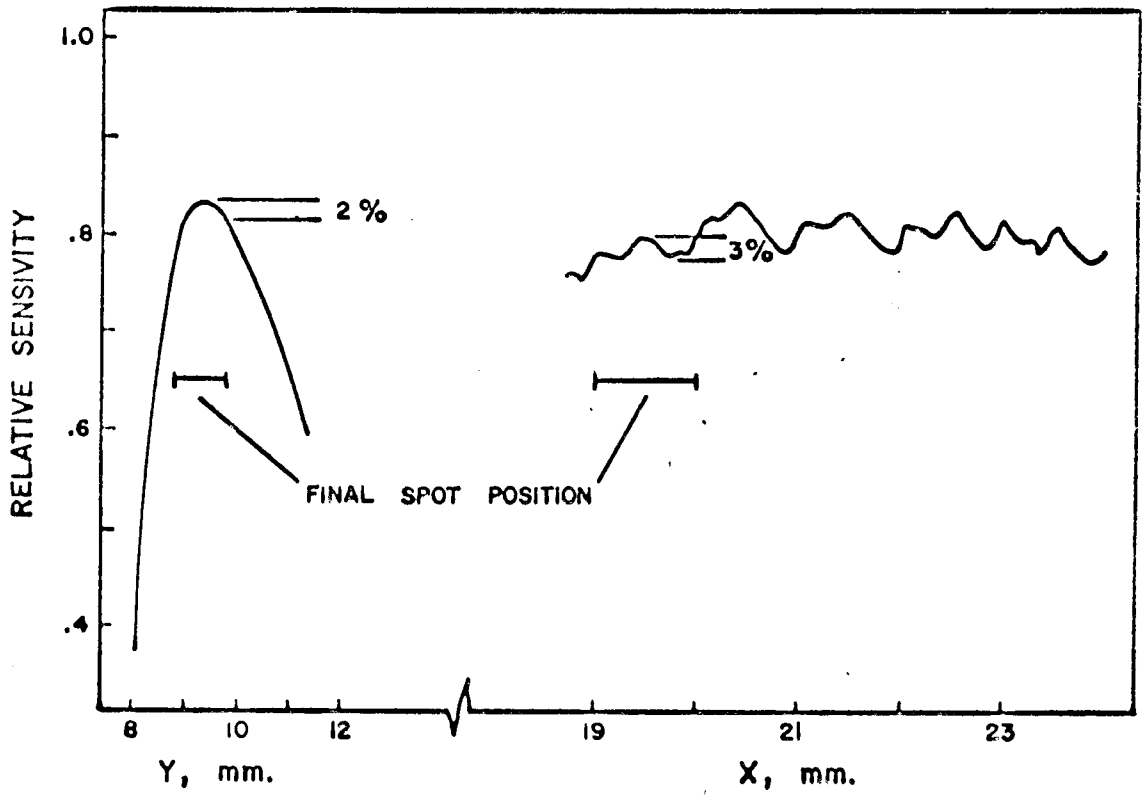

FIGURE 21. PHOTOMULTIPLIER (1P28) SENSITIVITY

was such that the photomultiplier could also be moved relative to the collecting lens (called the Z direction here) by a manual adjustment thus providing different spot sizes.

The optimization of position consisted of preliminary scanning in the X direction at various Z settings to get the best spot size at the grill. Then scanning in the Y and finally X directions yielded reproducible readings. At this point the photomultiplier was clamped rigidly.

In order to further increase the accuracy of the system it was decided to actuate the mirror, M_o, with a motorized magnet traverse mechanism to insure that the details of its movement were exactly the same each time.

In general the reflection of the shutter-mirror (I_A), the worst offender, was reproducible to approximately 0.5% rms deviation.

The reproducibility for the 2482 Å line was not as good but this was to be expected since reflectance and transmittance are more easily influenced by surface films and bulk inhomogeneity of the quartz flats.

METAL SOURCE

MOLECULAR BEAM OVEN The second basic system of apparatus was the metal source which consisted of a tantalum oven flinging a beam of antimony molecules at the quartz substrate. Perhaps the best development of choice of evaporation technique lies in describing the methods available.

The most obvious choice is evaporation from a heated filament. Although this has the advantages of ease of construction and operation plus negligible outgassing, the metal capacity is small and the flux of molecules is unpredictably nonuniform. Accurate incremental control of evaporation rate is extremely difficult. The use of a boat source eliminates most of these disadvantages but requires a vertically oriented system and heavy current vacuum feed-throughs leads.

The oven source finally used seemed most practical since it combined the advantages of all of the above methods with the capacity of a relatively enormous quantity of metal and the convenient use of an rf induction heater as a power source. The output flux of this device is well known (a Knudsen or cosine distribution) and can be made quite constant in time with careful temperature control.

A fourth alternative was the electron beam evaporator which promised to eliminate the last disadvantage of the other systems, the possible introduction of impurities from the crucible material. Also there is the possibility of greater control of evaporation rate. All this must be paid for in complexity, difficulty, and expense of construction however. Considerable experimental work (including the design and construction of a Pierce electron gun) was done on this method but problems of beam intensity, focus, and current stability did not permit its use.

Purity of the film was perhaps the most important consideration other than system practicality and included two aspects: 1) the maintainence of the highest possible vacuum and 2) source purity.

Comparison of simple evaporation rates shows the impurities introduced by the tantalum oven to be negligible since at the operating temperature (about 600°C) the vapor pressures differ by a factor of $\sim 10^{-29}$. To my knowledge this does not preclude the possiblity of lower evaporation temperatures for inter-metallic compounds. No attack on the tantalum was observed during extended operation of the oven however.

Uniformity of film thickness requires increasing the effective source-film distance to a sufficient value of using various extended source methods which do not lend themselves to the use of a large quantity of metal or incremental control of thickness. The conditions for optimum oven operation demand a small aperture (~ three-mm dia.) which is essentially a point source. Construction details dictated a

film-source distance of ~ 38 cm which results in a calculated thickness variation of ~ 1/8% but also demands a large quantity of evaporant. A limiting aperture in the path kept the system clean by defining the beam on an area slightly larger than the size of the quartz flat.

The use of an oven or any beam source with considerable thermal inertia requires the use of a shutter to define evaporation time. The shutter also served to isolate the source during outgassing and trial runs. The forward and back motion of the shutter used produced a nonuniformity in thickness of the film proportional to ratio of the time of shutter travel to the time required to produce a thickness increment. For a typical build-up rate of 0.5 Å per second and a film increment of 5 Å this produces a nonuniformity of about 2%.

If the mean free path of molecules inside an oven is large compared to the radius of the aperture, r, and the area of evaporant is $> 10\pi r^2$, molecular flow conditions are satisfied. For low pressures the efflux is a Knudsen distribution given by:

$$\Gamma \text{ , } \frac{\text{g.}}{\text{sec. steradian}} = Cr^2P\left(\frac{M}{T}\right)^{\frac{1}{2}} \cos\theta \qquad (27)$$

where $C = 5.85 \times 10^{-5}$

r = aperture radius, cm

M = molecular weight

P = vapor pressure in microns at T°, K.

θ = polar angle

1 micron = 10^{-3} Torr

The vapor pressure in microns at T^{o} K is given by:

$$\text{Log}_{10} p = -\frac{B}{T} + A .$$

Dushman gives the following values: A = 11.15 and B = 8.63×10^{3} degree Kelvin for antimony (9). As the vapor pressure is increased by raising the temperature the mean free path is rapidly decreased requiring a smaller aperture and hence tending to decrease output flux under the molecular flow restriction.

Computations made for the design of the oven were based on vapor pressure data taken from the Handbook of Chemistry and Physics (41st Edition), but this data was found to be in error by over an order of magnitude (determined by film build-up rates and verified in reference (9)). Fortunately the system still worked but at a much lower temperature than expected.

Figure 22 is a schematic of the oven design. Note that the thermocouple leads are brought out to a rather long stem which could easily be

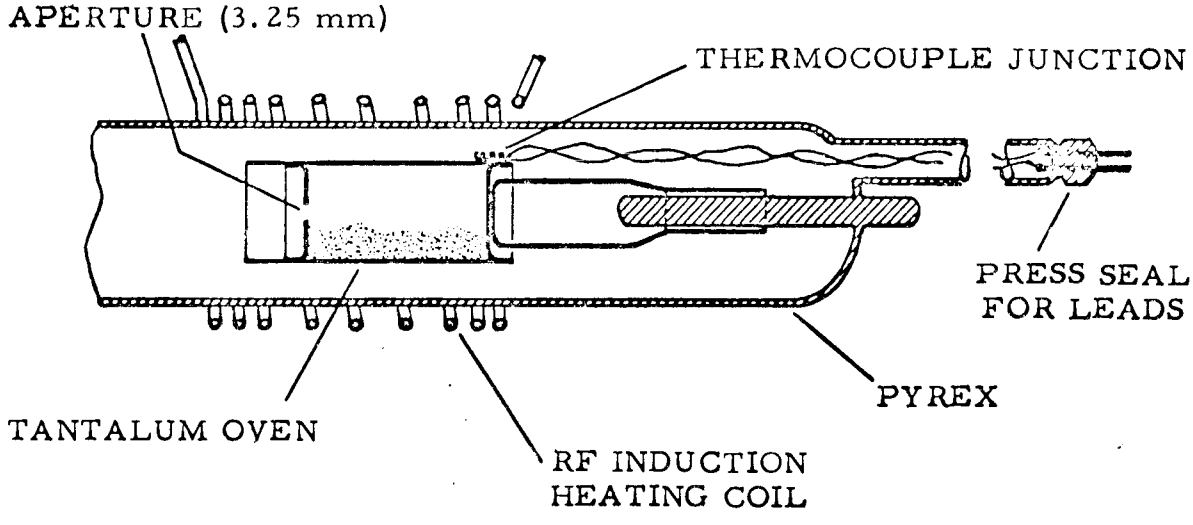

FIGURE 22. MOLECULAR BEAM OVEN

kept at room temperature to avoid unknown emf's at the glass to metal seals. Thermocouple calibration was checked against a pyrometer at somewhat higher temperatures than those used (700°C - 950°C) and the thermocouple was consistantly ~ 6% lower. Film build-up rates seem to indicate the correctness of the pyrometer. The reason for this was probably slight evaporation of the thermocouple alloy constituents during high temperature tests and outgassing.

The oven was tested and outgassed on a separate high vacuum system where evaporation rates were estimated visually by opaque film build-up times. Put on the experimental tube with a 10 gram charge of Sb (as a coarse powder), the oven required some 50 hours of outgassing at slightly below evaporation temperatures. The evaporation rate used varied from 0.2 to 0.9 Angstroms per second. Tube pressure during evaporation was less than 10^{-7} Torr.

FILM THICKNESS DETERMINATION On the optical transmission (t) versus film thickness (τ) curve (see Figure 13) there are two areas of greater reliability since: 1) The first portions of the curve near $\tau = 0$ are sensitive to zeroing corrections and nonuniform tube operation, 2) the central portion from $\tau = 80\text{Å}$ to $\tau = 140\text{Å}$ has two possible thickness values depending on the film's structure and 3) the final portion for $\tau > 240\text{Å}$ is very insensitive to thickness changes since $t^2 < 0.01$. Because of these intervals of uncertainty in the thickness data as derived from optical parameters, it was decided to use evaporation rate data to extrapolate through these areas.

At film No. 30 the substrate was raised to room temperature and there were various indications that the crystalline form had been obtained. It was decided to use film No. 36 (τ = 203Å) as an absolute value of film thickness. The extrapolation was made to join the other reliable portion of the optical parameter curve by a linear adjustment of the thermocouple voltage-temperature relation. Using a trial evaporation rate from the optical curve slope around film No. 36 the evaporation equations give a temperature, T_e, which was used to adjust the termocouple reading by the use of

$$T = \frac{(\xi - \xi_o)}{(\xi_e - \xi_o)} T_e \cdot \qquad (38)$$

(Here a thermocouple emf ξ gives a temperature T^o, C. where ξ_o is the emf at the ice-point and ξ_e is the emf for the trial temperature T_e). The "theoretical" evaporation curve was then used with experimental oven parameters and the derived temperature to numerically integrate film thickness to the region 40Å < τ < 60Å on the optical parameter curve.

After several trials this extrapolation provided a remarkable fit to the optical data as shown in Figure 23. In view of the resulting curve, the structure transformation of film No. 30 seems quite well based. The evaporation rate values were used as final thickness--film number relations in all regions except the first seven films where oven operation was not regular enough to yield reliable values.

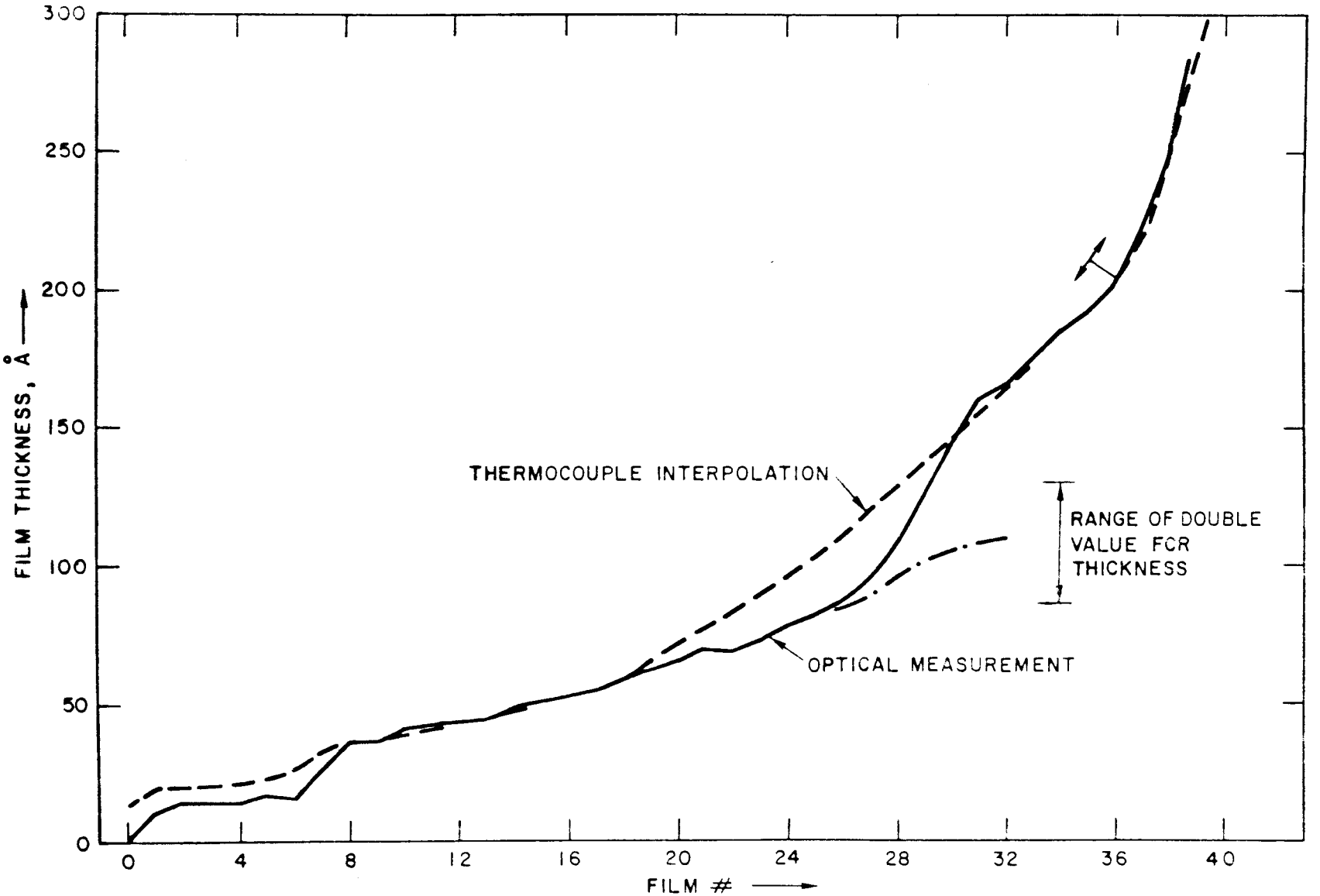

FIGURE 23. FILM THICKNESS VERSUS FILM NUMBER

For a thermocouple reading of 22 mv. the handbook temperature is 560°C and the pyrometer temperature was 615°C. Since the temperature would have to be known to ~ 0.06% for 1%-thickness knowledge, it is clear that the use of temperature data alone would be quite inaccurate. Chemical methods (polarographic techniques and colorimetry) can be used to determine the final thickness to ± 1% with careful analysis (18).

PHOTOCURRENT MEASUREMENT

To measure the minute photocurrent from the antimony film (on the order of 10^{-14} amp) a vibrating reed electrometer was used. This instrument makes an essentially infinite impedance measurement of the voltage across a specially constructed capacitor yielding a recorder output which can be differentiated to obtain the current desired.

In the simplified circuit below (Figure 24) C_c is the measuring capacitor (10 μμf.), C_v is the vibrating reed capacitor whose capacity is changed at 435 cycles/sec, and C_2 is a coupling capacitor to the feedback circuit. Any voltage across C_v acts through the feedback amplifier to adjust V in such a way that the voltage across C_v is reduced to zero. Then V is essentially the voltage across the measuring capacitor and $Q = C_c V$.

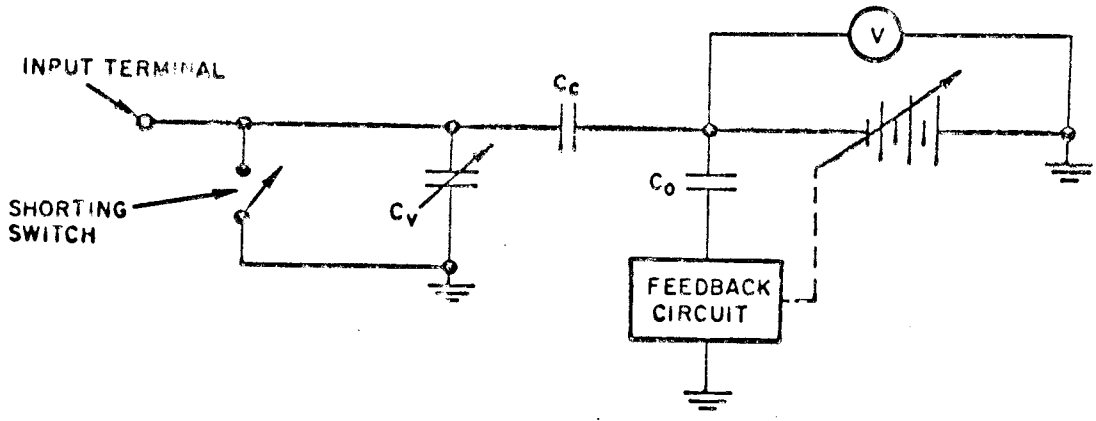

FIGURE 24. SIMPLIFIED ELECTROMETER CIRCUIT

The electrometer input connection and substrate support were built into a dewar arrangement in order to maintain the film at liquid nitrogen temperatures (Figure 25). The lead-in was supported at its lower end by a guarded uranium glass insulator and shielded by a coaxial nickel tube which was insulated from it by a pyrex tube. To mechanically isolate the electrometer input terminal a fine wire spring was used to connect the upper end of the lead-in. The lead itself had sufficient length above the coolant level for thermal insulation.

The stem was evacuated, baked-out at 420°C and then re-evacuated and sealed to eliminate moisture films on the insulators. At this point the measured resistance was about 10^{13} ohms at room temperature.

Due to the extreme sensitivity and low impedance of the electrometer, elaborate care was necessary to electrically shield all sensitive parts and to prevent extraneous charge movement. In the final

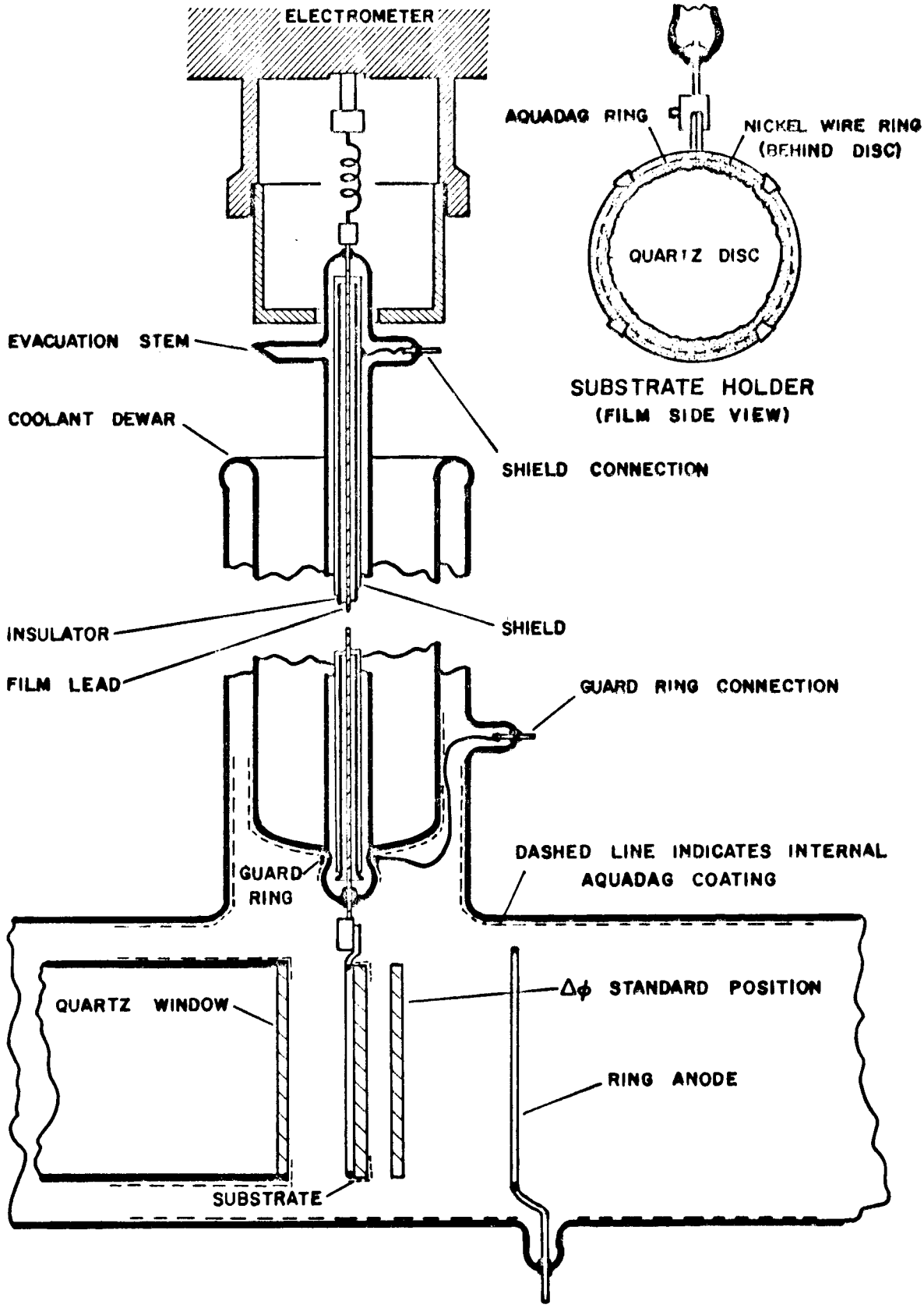

FIGURE 25. SUBSTRATE HOLDER AND ELECTROMETER LEAD

version of the tube this was accomplished by coating as much of the inside of the tube as possible with Aquadag.[7] This also eliminated accumulation of charge on the glass surface. (Trouble with internal charge movement was experienced during the first run when the tube was externally shielded.) The Aquadag coating and all metal parts within the tube were connected to external grounds.

To prevent polarization of the substrate support insulator a guard ring of nickel wire and Aquadag surrounded it and was connected to ground. Thus the voltage across this insulator was essentially the contact potential existing across the vibrating reed capacitor of the electrometer (about 30 mv.).

A steady background or drift current due to contact differences of potential, thermoelectric emfs, dielectric absorption currents, and insulator stresses (induced thermally or mechanically) is measured by the electrometer. Before installation on the tube a drift (i_d) current of 2×10^{-17} amp. (with the input terminal shielded) indicated proper operation. Normal drift current on the tube was quite high but upon cooling the stem it reduced to about 10^{-15} amp. Using the existing contact potential across C_v this indicates an insulation resistance of $\sim 3 \times 10^{13}$ ohms.

To collect the photocurrent a ring anode 4.5 cm in diameter of 0.040 inch nickel wire was positioned coaxially 3 cm from the cathode

---

7. Acheson Colloids Company's water dispersed colloidal graphite.

surface. It was held at 55 volts during current measurements. For the parallel plate energy distributions the $\Delta\phi$ standard was used as an anode. In this case the interelectrode distance was 1.85 mm. The i_p measurement usually consisted of a charge accumulation over 3-4 minutes preceded and followed by a drift current accumulation of the same length.

WORK FUNCTION MEASUREMENT

The work function measurement might be thought of as a slow-moving vibrating capacitor electrometer controlled by human feedback. If we form a capacitor from the antimony film and a standard gold film a contact potential equal to the difference in work functions for the two metals exists across the shorted capacitor. By varying the inter-film distance periodically[8] a charge wave whose amplitude is proportional to contact potential ($\Delta\phi$) and the change in capacitance is seen by the electrometer connected across the films. A series voltage source was introduced to null out the charge variation and the work function difference could be read directly (see Figure 26).

Plotting charge variation amplitudes against various external nulling voltages to obtain a null graphically was found to be more

---

8. Interfilm distance = 2.85 $\pm$ 1.05 mm.

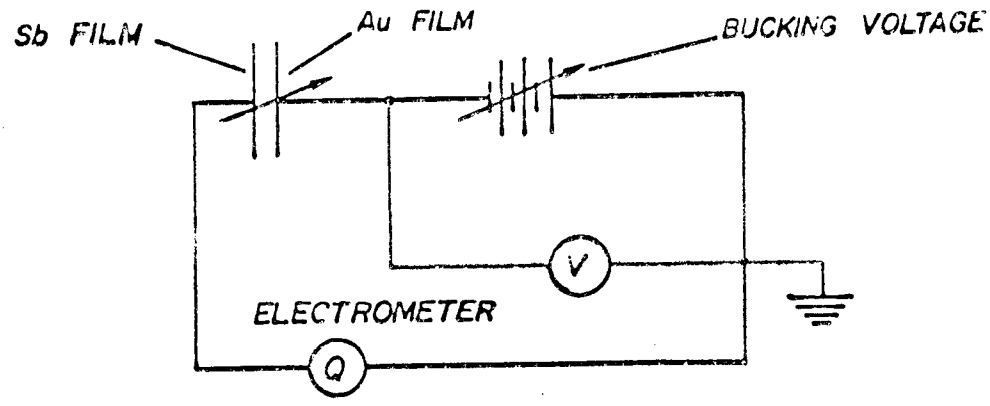

FIGURE 26. WORK FUNCTION MEASUREMENT

accurate as well as saving precious time during the experiment. The actual null amplitude did not reduce to zero until the final films were laid down, an effect which is presumed to arise from the resistivity of the film.

By varying the voltage between the film and any other tube electrode interelectrode capacitances could easily be determined. With the gold film in closest position the capacitance between it and the substrate served as a measure of film resistivity. (Initially C_f = 3.1 pf. and finally C_f = 6.9 pf.)

MISCELLANEOUS ASPECTS

VOLTAGE SUPPLIES Measurement of work function differences required a one volt voltage source of good precision while for photoemission a fifty-five volt source of excellent stability was required. The two sources were "overlapped" in the final voltage supply circuit (see Figure 27).

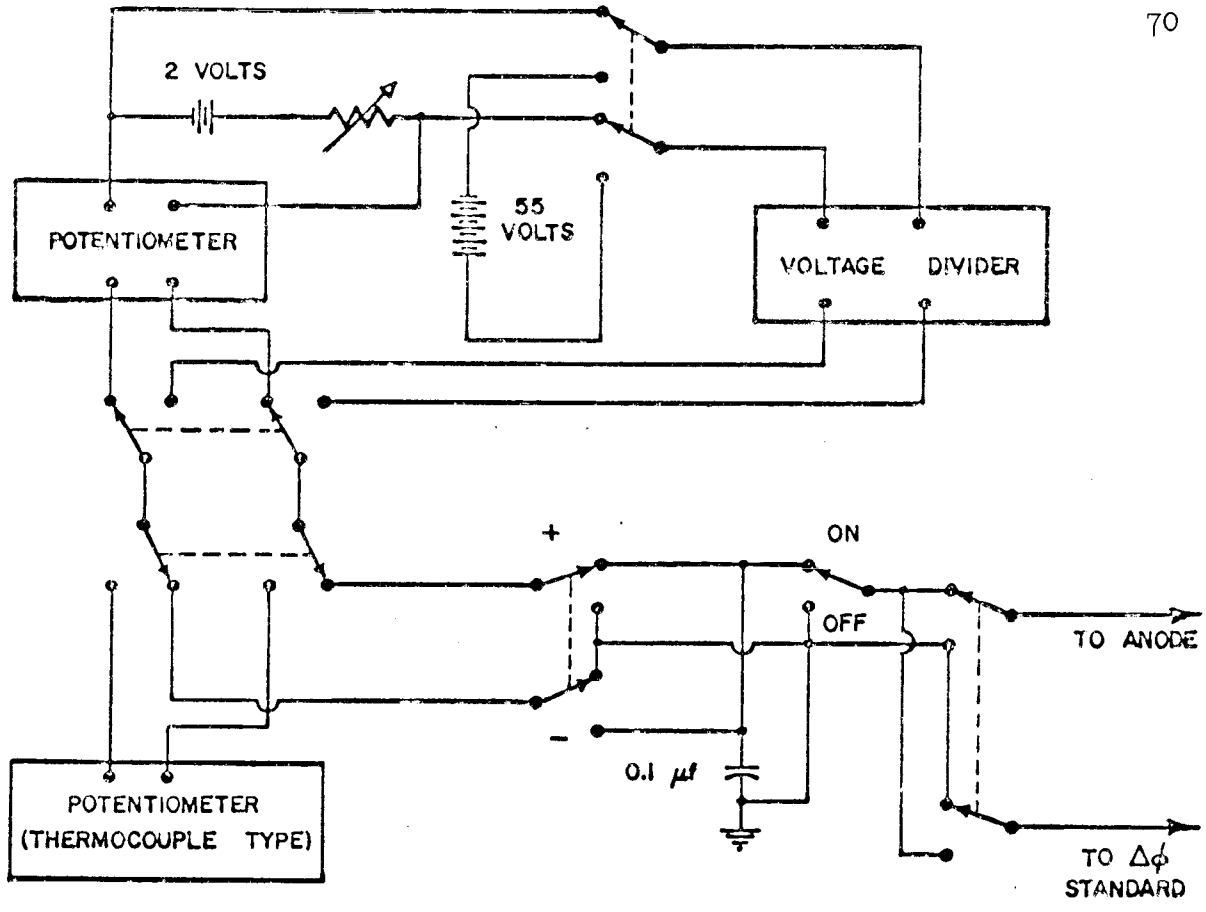

FIGURE 27. VOLTAGE SUPPLY CIRCUIT

All critical leads were shielded and short-term fluctuations were shorted to ground by a large capacitor. Since the film and collector form a capacitance couple it was essential that the supply voltage be very stable. By using large storage batteries a drift of less than 10^{-6} volt/second was obtained.

Voltage standardization was done using a standard cell potentiometer circuit. Since it was intended for thermocouple use its maximum was 80 mv and it was used in connection with a precision voltage divider.

SUBSTRATE An optically polished fused quartz disc 3.8 cm. in diameter by 0.16 cm. thick was mounted on a dewar as shown in Figure 25 where it could be maintained at constant temperature.

After a detergent wash the disc was soaked in hot chromic acid, then a thirty-second rinse in 25% HF and many rinses in double distilled water followed. The flat was baked to 850°C in an electric muffle furnace in air and finally inserted in its holder a nickel wire ring with metal tabs, to hold it securely. After ringing the flat with Aquadag several times to insure good contact the assembly was baked again at 300°C in air to volatize as many impurities in the Aquadag as possible. A black breath figure[9] was evident at all times following the water rinses.

The holder was inserted in the tube through a side port and aligned by its optical reflection. Tightening the setscrew and testing for conductivity (< 500 ohms to a point contact) completed the installation.

GOLD STANDARD FILM In order to place a gold standard film before the substrate, vibrate it and then remove it from the light path, a slide pivot arrangement was built (Figure 28). Slides were of tungsten rod lubricated with Aquadag moving in stainless steel tubing. Pivots were of the same materials and the arrangement was constructed of pyrex rod and various sealing glasses. A glass encapsulated iron slug provided means of moving the slide magnetically and glass bellows provided the flexibility to vibrate the gold film.

---

9. A microscopically clean surface, free of oil films, will not fog when breathed upon since condensed moisture forms a continuous film.

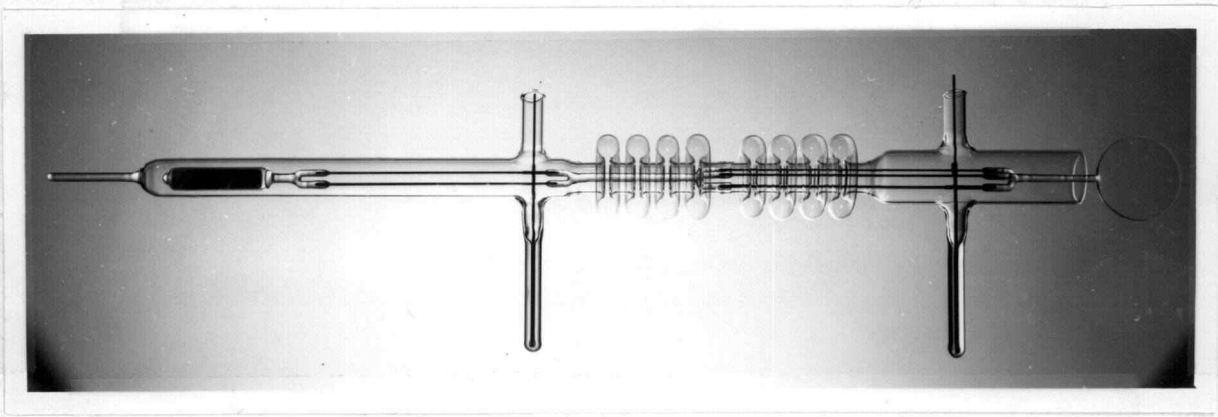

FIGURE 28. $\Delta\phi$ STANDARD MOVEMENT

The gold film was evaporated on a quartz flat identical with the substrate using a tungsten filament source which faced the flat in its retracted position. This evaporation was carried out just prior to the beginning of each film series at pressures in the 10^{-7} Torr range.

A motor driven, variable stroke eccentric was used to drive the film capacitor at a constant rate. It was adjusted to give a film separation of 0.39 cm. maximum and 0.18 cm. minimum.

ENVELOPE AND VACUUM SYSTEM Despite the danger of breakage and the difficulty of assembly, pyrex construction was considered the best because of the ease of producing vacuum seals and relatively inexpensive construction.

All glass parts were annealed at $> 500^{\circ}C$ in air before final assembly giving quite clean surfaces. A filtered argon flush provided a slight positive pressure to prevent flame from entering joints during sealing.

To produce a clean, oil-free vacuum in the 10^{-9} Torr range a VacIon[10] pump (8 liters/sec) plus a liquid nitrogen trap was used. Pressure as indicated by pump current showed good agreement with a standard ion gauge in a pre-experiment test. After the tube was rough-pumped through two liquid nitrogen traps it was sealed off with a glass-blown seal. All joints except the copper gasketed flange at the pump were glass-blown seals.

Since the entire tube was baked-out at 420°C before the first run it was constructed on an iron frame so that it was semi-portable and could be placed inside the annealing oven used for bake-out. Although the bake-out did not substantially change the ultimate vacuum attainable, a huge amount of water vapor was removed from the tube. This appeared as ice in the cold trap and almost 14 hours of pumping at around 10^{-4} Torr (the maximum continuous pumping pressure to avoid overheating the pump) were required to clear the trap. Because of the danger of breakage involved in oven bake-out it was decided to use heating tapes at around 200°C for later runs.

---

10. Varian Associates trademark for their sputter-ion pump.

VI. RESULTS AND CONCLUSIONS

For small film thicknesses the high resistivity of the film made unambiguous measurements impossible so that only a qualitative analysis could be made. At higher film conductivities quantitative photocurrent and contact potential data was taken and energy distributions were determined and compared with the Fowler-DuBridge theory. A theory for the total photocurrent as a function of film thickness (for light emergent geometry) is advanced and compared with experimental data.

TUBE OPERATION AND DATA

Most aspects of tube operation have been covered individually under the heading of apparatus. The remaining topics will be discussed here as they are related to the tube's operation schedule. On a typical numbered film (particular film thickness) the following operations were done:

Equipment check - Zeroing of recorders, initial data.

Evaporation - According to oven preheating sequence.

$\Delta\phi$ measurement - Including potentiometer standardization and battery voltage measurement.

Interelectrode capacitance measurement

Optical properties - Reflection and transmission coefficients at λ_t and λ_p.

Photoemission measurement - Determined with and without light incident. (Drift current)

Brief analysis - Calculation of approximate $\Delta\phi$, τ, and photocurrent. Adjustment of oven heating sequence.

Most of the 41 film thicknesses of the final run followed this schedule which took about an hour to complete. However, occasional reruns of parts of the sequence were done when long time lapses and/or temperature changes occurred. Many extra photocurrent determinations were done to determine stability and decay rate. After a stable photocurrent was obtained several energy distributions were done using both the ring anode (at constant voltage for all photocurrent versus film thickness data) and the $\Delta\phi$ standard film as an anode (a good approximation to plane-parallel plate geometry). Over the whole series the average time per run was around two hours.

Although the first series of 34 films yielded no usable quantitative data it did show that the film remained highly resistive for thicknesses of at least 70 to 80 Å. Several modifications of the experimental tube were indicated and are summarized below:

Photocurrent measurement - The high and unstable electrometer drift current suggested that an internal electrostatic shield was necessary to prevent accumulation of static charges on the glass surface. Incident light intensity was increased for a more favorable signal to noise ratio.

$\Delta\phi$ measurement - The graphical interpolation method for null determination (see apparatus section) and the measurement of inter-electrode (film-Au standard) capacitance were developed during the first run. Various tests were run to check the operation and linearity of the contact potential system with an inserted continuous film before the final run.

Abnormal $\Delta\phi$ voltages of +6 to -6 volts indicated the presence of large static charges and further demonstrated the high resistivity of the film.

Thickness measurement - In order to improve reproducibility of the internal mirror response an automated mirror movement was constructed and installed.

Metal source - The molecular beam's erratic behavior suggested that the evaporant temperature was not stabilized during the evaporation period. A longer preheat cycle was instituted.

Prior to the second series of films all the recommended modifications were accomplished. The inside of the tube was carefully coated with Aquadag in several layers until the resistance to the external connection was < 400 ohms to a point contact placed anywhere on the shield (coating indicated in Figure 24). At atmospheric pressure the drift current, i_d, ranged up to 12 fa.[11] with the shield and electrodes grounded. Upon evacuation to 200 Torr this went to -2 fa. and behaved

---

11. One femptoamp = 10^{-15} amp.

quite erratically. Moisture and NH_4OH in the Aquadag coating seemed responsible. Using a trapped forepump to reduce the pressure to < 0.01 Torr stabilized the drift current even when the collector voltage was varied from -54 to +54 volts.

Cooling the tube dewar with dry ice again caused instability and great sensitivity to vibration. Finally time, and a better vacuum, cured this and the drift current became stabilized with $1.0 < i_d < 1.2$ fa. (This value is still large compared with a capped head electrometer drift current of 0.06 fa.)

To test the $\Delta\phi$ measurement an Aquadag covered substrate was mounted in the tube yielding a $\Delta\phi$ of 64 ± 1 mv (with the Au film positive) at room temperature. This test was run with a makeshift substrate whose alignment with the Au standard was poor however and there was some sensitivity to shield voltage (10 mv/volt).

Series Two Results. The data obtained in series two were in most respects more stable and are felt to reflect more accurately the properties of the film. In Figure 29 is presented data on i_p, $\Delta\phi$, and C in terms of film number drawn so as to indicate changes occurring between thickness increments and those occurring during measurements and those occurring during measurements on one film. Figure 30 shows $\Delta\phi$ and i_p plotted versus film thickness.

From the second film onward it was evident that the observed i_p was decaying with time but since the system behaved well the experiment was continued even when i_p dropped to zero near film No. 13 (50Å).

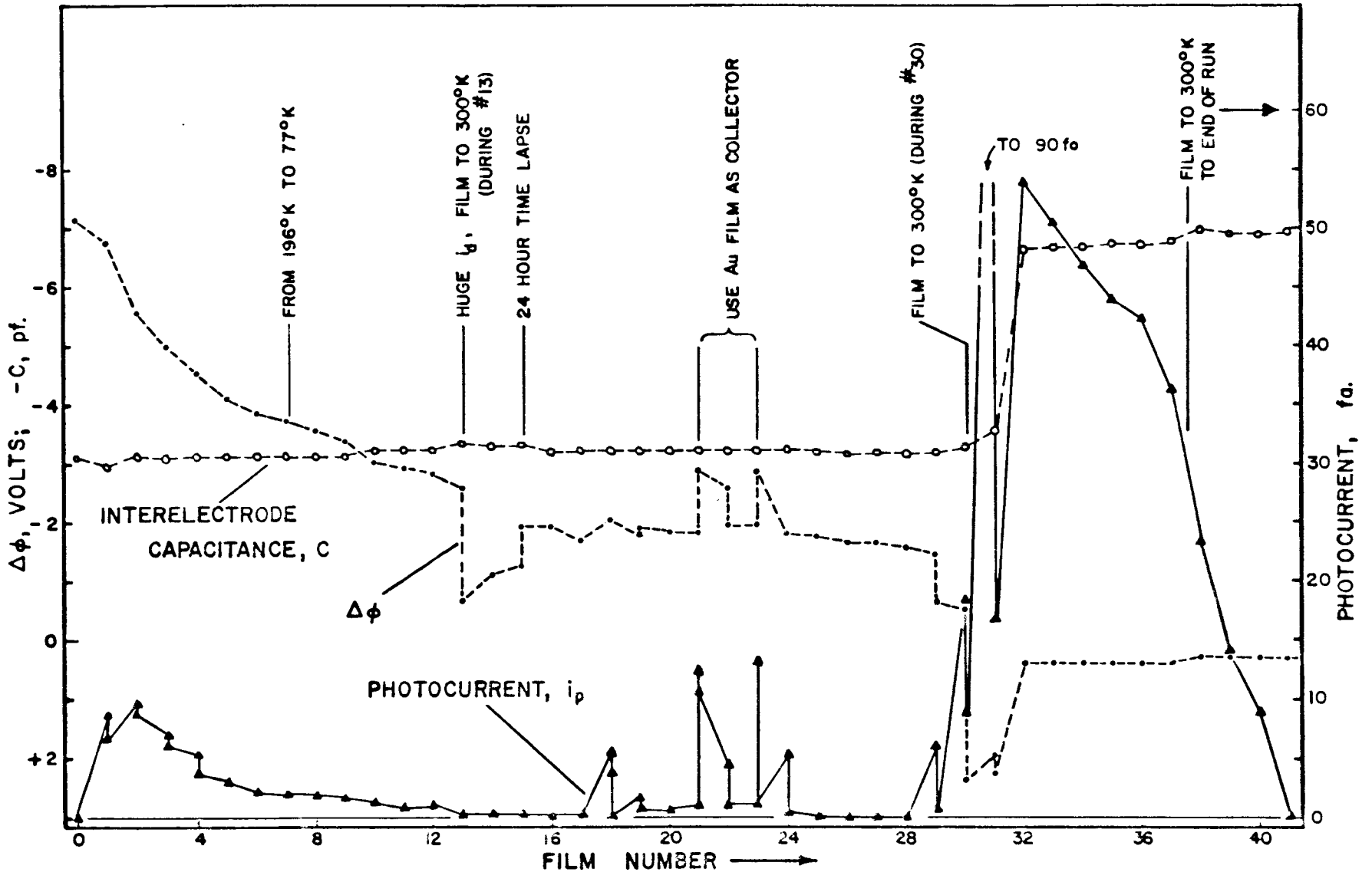

FIGURE 29. FILM PROPERTIES VERSUS FILM NUMBER

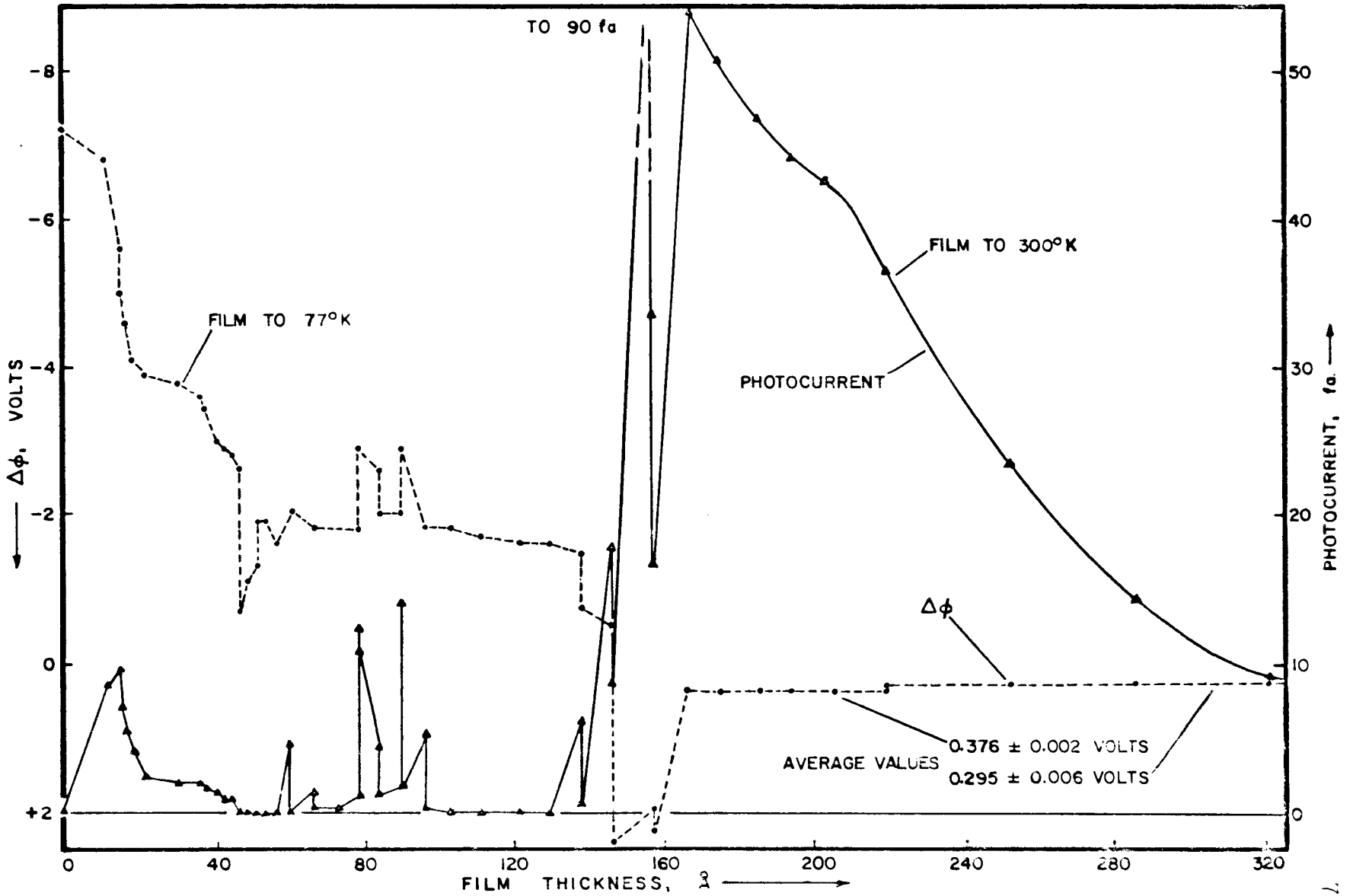

FIGURE 30. FILM PROPERTIES VERSUS FILM THICKNESS

Prior to film No. 8 the dry ice coolant was replaced with liquid nitrogen (supersaturation of CO_2 in the acetone-dry ice mixture made boil-overs frequent). Although the rate of decay of photoemission with film thickness increased slightly no other changes were noted as the temperature change.

During the 13th film the electrometer drift current abruptly became erratic, reversing in sign and increasing to ~ 15 fa. With the addition of coolant it became positive again but soon went more than 175 fa. negative. During the next 48 hours the equipment was thoroughly checked. No consistant pattern could be found in its chaotic behavior. The substrate was raised to near room temperature inadvertantly but even this produced no permanent improvement. Charges of more than 600 picocoulombs were being transferred. After some ice was removed from the dewar the i_d became more normal. Because of the time correlation it is probable that piezoelectric currents due to ice expansion in the dewar caused the instability. The drift current remained erratic on a smaller scale through film No. 20 (~ 70Å) with values ranging from -0.1 to +1.4 fa.

At film No. 29 there was measurable photoemission but it decayed rapidly to zero. During No. 30 the film was raised to room temperature for a short time to silver the inside of the dewar. This reduced the rapid boil-off of liquid nitrogen and improved drift current stability by additional shielding. At this thickness $\Delta\phi$ changed sign and the

photocurrent, i_p, decayed to a nonzero value. After film No. 37 room temperature data was obtained for the remainder of the experiment.

At the termination of series 2 experiments it was apparent that rather extensive modifications would be necessary if the work was to be continued in a meaningful direction:

a) The glass blown seal on the substrate changing port could safely permit only one more seal off which was reserved for the installation of a demountable metal gasket seal. (Each time a sealing operation is done a certain amount of devitrification of the pyrex takes place.)

b) In order to obtain energy distribution data of sufficient accuracy the photocurrent to drift current ratio would have to be improved.

c) The problems involved with building up a conductive film would have to be surmounted in order to make low thickness measurements.

INTERPRETATION AND ANALYSIS OF RESULTS

NON CONDUCTIVE REGION The expected increase in photocurrent from zero is shown by the first two films due to increasing absorption of light. Although it is probable that the film's growth is by way of agglomeration into small patches it is impossible to be more specific about the details of structure from these data. However, some decay of photoemission with time indicative of a nonconductive film is already evident in the first two films.

Examination of the consistant pattern of decay of photocurrent (i_p) with both time and film number during the next eleven film thicknesses indicates that i_p is a function of the amount of charge leaving the substrate rather than an explicit film thickness effect.[12] This is deduced from the following:

a) A plot of i_p vs. $\int i_p dt$ yields a good fit to an exponential decay curve with a discontinuity in slope at film No. 7 when the temperature was changed from 200°K to 77°K.

b) The major portion of decay of i_p for a particular film takes place during photoemission.

c) A plot of i_p vs. τ shows no simple relationship.

The initial contact potential measurement indicated an incredible 7.15 volts (before the first film)[13] with the substrate charged negatively (favoring photoemission). During the first thirteen films photoemission reduces this negative charge to a degree which depends on the external electric field used for electron collection. This change in the charge distribution on the nonconducting film finally reduces photoemission to zero.

---

12. An effect based on change of structure or thickness.

13. The $\Delta\phi$ value was essentially the same as 24 hours before the beginning of series 2.

If the film is nonconducting, the electrometer does not record photoemission currents but rather charge flow to ground from the periphery of the substrate resulting from change in charge distribution on the substrate. Note that the electrometer is connected to an Aquadag ring on the substrate surface (Figure 25). This makes more plausible the seemingly contradictory situation in which the $\Delta\phi$ measurement indicates a negative charge on the substrate while photoemission is inhibited completely.

Although the work function measurement is a rather involved electrostatics problem under these circumstances it can be intuitively explained as follows: The substrate consists of a conductive ring surrounding an insulated disc upon which the Sb is deposited. A conductive plane (the Au standard film) is moved up to 3.4 mm of it and wiggled. (See Figure 25 and the section on work function measurement, p. 68.) Ordinarily, the constant voltage across conductive capacitor plates produces a charge displacement in the electrometer circuit as electric field is varied by the capacitance change. When this field is nulled out we know $\Delta\phi$.

In the nonconductive film situation however, the major portion of the film plane is insulated so charge displacement in the electrometer circuit must be accomplished by a redistribution of charge on the ring surrounding the insulated portion. Nulling then becomes a process of minimizing the effect of plate separation on the electric field

configuration between the plates. This is possible because the field shape is highly dependent on the voltage impressed on the $\Delta\phi$ standard.

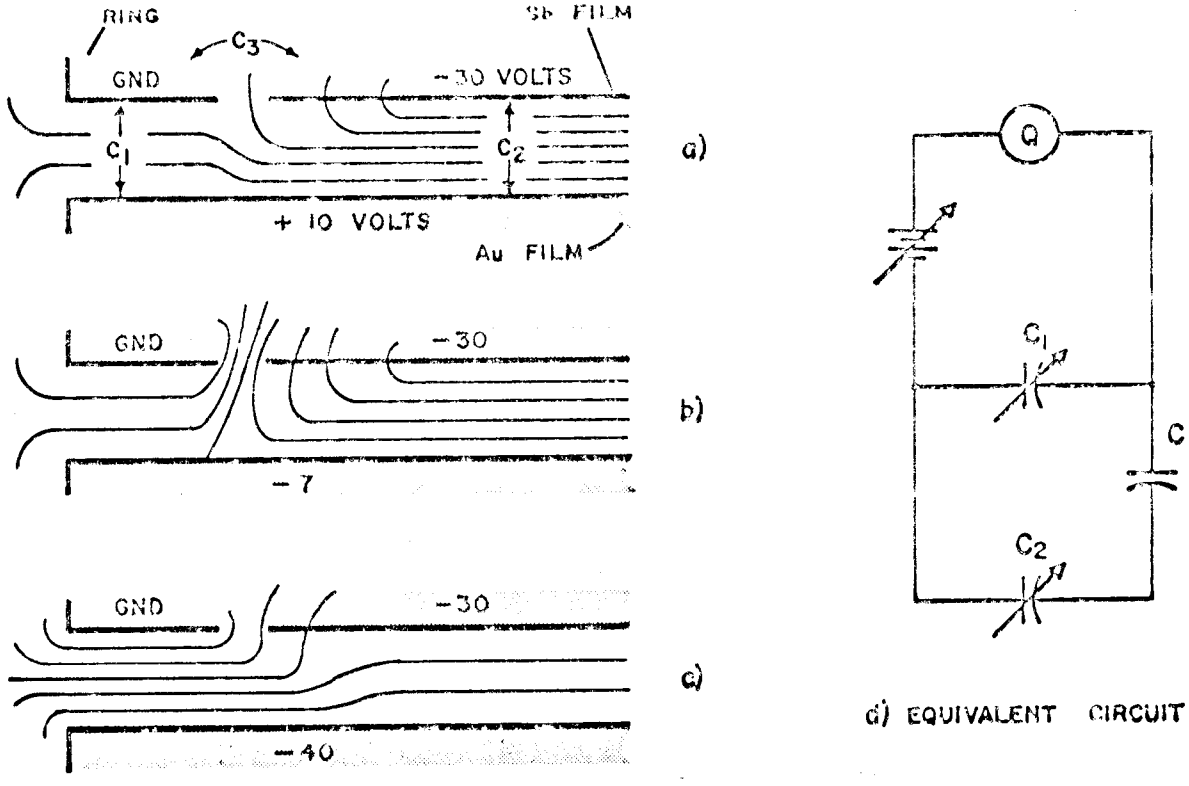

FIGURE 31. EQUIPOTENTIAL MAP FOR $\Delta\varphi$ MEASUREMENT

From a charge conservation standpoint it is apparent that for situation a) in Figure 31 charge flows from both C_1 and C_2 by increasing the plate separation. Also in situation c) charge flows from both C_1 and C_2 when plate separation is increased. For some Au film voltage (substrate ring at ground potential) there will be a field configuration (b) such that the charge flow from the ring is balanced by the charge flow from the Sb film - Au film system. Since the ring is capacitively coupled to the Sb film (C_3) a relative null is exhibited

in the electrometer reading at this point. Additional support for the preceding hypothesis comes from the reduction of null amplitude exhibited after the film becomes conductive.

The electric field configuration is quite different during photoemission and the problem is to explain the degradation of photoemission from an apparently negatively charged substrate. At his point the situation may be summarized by these statements:

1) The substrate appears to be highly negatively charged initially.

2) The anomalous contact potential measurement can be explained as a field configuration dependent phenomena.

3) We have assumed that the film's saturated photoemission is not affected by electric fields of the magnitude encountered here (i.e., a Schottky type effect is not in operation here.)

4) The decay of i_p is ultimately dependent on $\int i_p dt$, the photocharge, but the causal relationship of the magnitude of $\Delta\phi$ is not obvious.

The problem then reduces to one of reconciling the i_p decay and the $\Delta\phi$ measurement. Photocurrent decay as a result of electric field dependence of the properties of the film (i.e., a change in the effective work function or tunneling effects between patches is unlikely with the fields involved (5, 12)). The inhibition of photoemission by a structure dependent threshold whose proximity to the exciting wave length makes emission highly sensitive to external field conditions is ruled out since the major portion of i_p decay occurred not between films but during emission.

From the above discussion it is apparent that i_p decay and the anomalous $\Delta\phi$ measurement are the direct result of film resistivity. Electrons emitted from isolated patches of antimony can reach the collector until the patches become positive enough to inhibit photoemission. Measured photocurrent is due to electric field redistribution around the ring surrounding the film. This hypothesis is supported by the interelectrode capacitance measurement which indicates a radical change in film resistivity which coincides with appearance of a non-decaying i_p and stable, normal $\Delta\phi$ values (see Figure 29). Although the patches are positively charged, the quartz substrate may be negatively charged enough to give a negative $\Delta\phi$ indication.

TRANSITION Further indications of photoemission appeared during the next seventeen films (before stable emission was obtained) particularly in the region around 80Å film thickness but emission decayed rapidly to zero in all cases. Other workers (7, 22) have reported a phase transition from amorphous to crystalline structure for Sb at 85Å and 150-300Å with dependence on the rate of deposition and substrate temperature. Optical data suggest that such a transition occurred around 150Å for this film. There is, however, optical evidence of anomalous behavior around 60-80Å. Certainly we can say that at film No. 30 (raised to ~ 27°C for dewar silvering) that some crystallization must have taken place.

For films No. 30 through No. 32 the deposition approached bulk conductivity quite rapidly as indicated by reasonable $\Delta\phi$ values, a stable i_p, and a definite jump in Sb-Au film interelectrode capacitance--all of which quickly assumed stable and predictable values. Stable-property film thickness was around 165Å. Although the heating of the layer to room temperature during film No. 30 probably initiated the onset of stable behavior this approach continued after the film was reduced to 77°K and was not completed until film No. 32 several hours later.

During this interval the $\Delta\phi$ indication changed to an abnormal negative value (~ 2.3 volts with the substrate positively charged) which is the expected behavior for a highly resistive but continuous film. The charge step for the interelectrode capacitance measurement became somewhat rounded in this thickness region which is also indicative of lowered resistivity enabling the film to play a part (although sluggishly) in the capacitance measurement. Photocurrent decayed to a nonzero value for the first time since film No. 13.

PROPERTIES OF THE CONDUCTIVE FILM For the remaining films (No. 32 through No. 41) all measurements were quite well behaved with photocurrent decreasing quite rapidly with increasing film thickness and $\Delta\phi$ remained quite stable.

When the film became conductive enough for a stable photocurrent energy distributions were taken on film No. 32 at 77°K and film No. 39 at 300°K using the Au film as a collector to approximate parallel plate geometry. Figure 33 shows the obtained photocurrent curves as a function of retarding voltage, V_r. The reverse photocurrent from

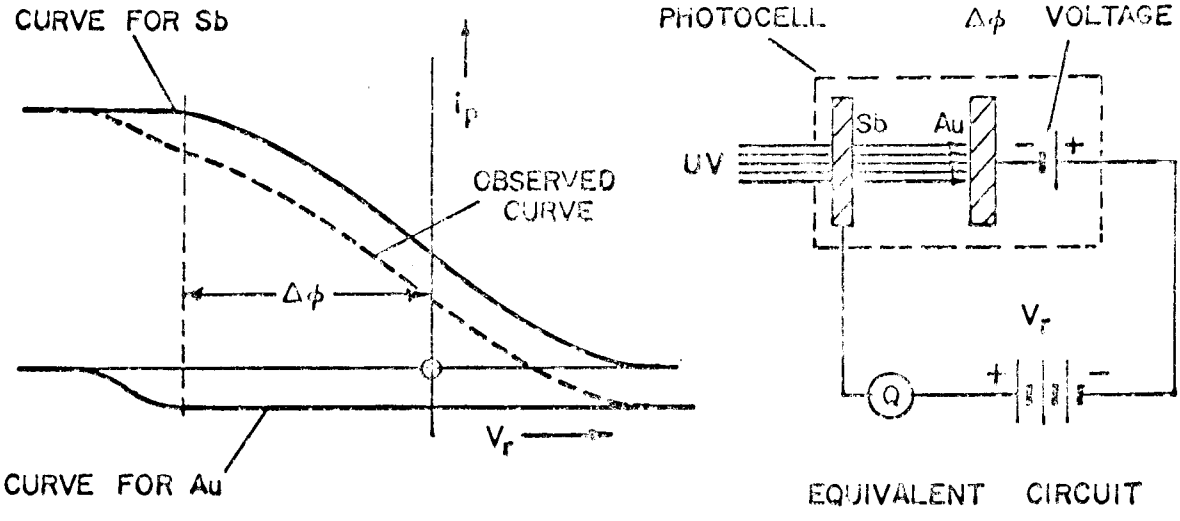

FIGURE 32. EXPERIMENTAL PHOTOCURRENT CORRECTIONS

the Au film was subtracted on the i_p versus V_r curve over the range on interest as shown in Figure 32. The obtained curves were translated by a voltage $\Delta\phi$ and then normalized by division by the saturated photocurrent. Slopes of these curves gave the energy distributions shown in Figure 34.

Appropriate portions of the i_p versus V_r curve were plotted (Figure 35) following the Fowler-DuBridge graphical method outlined in the theory section to yield values the work function which are shown in Table 4 ($V_m e = h\nu - \phi e$ = maximum energy of emission at 0°K).

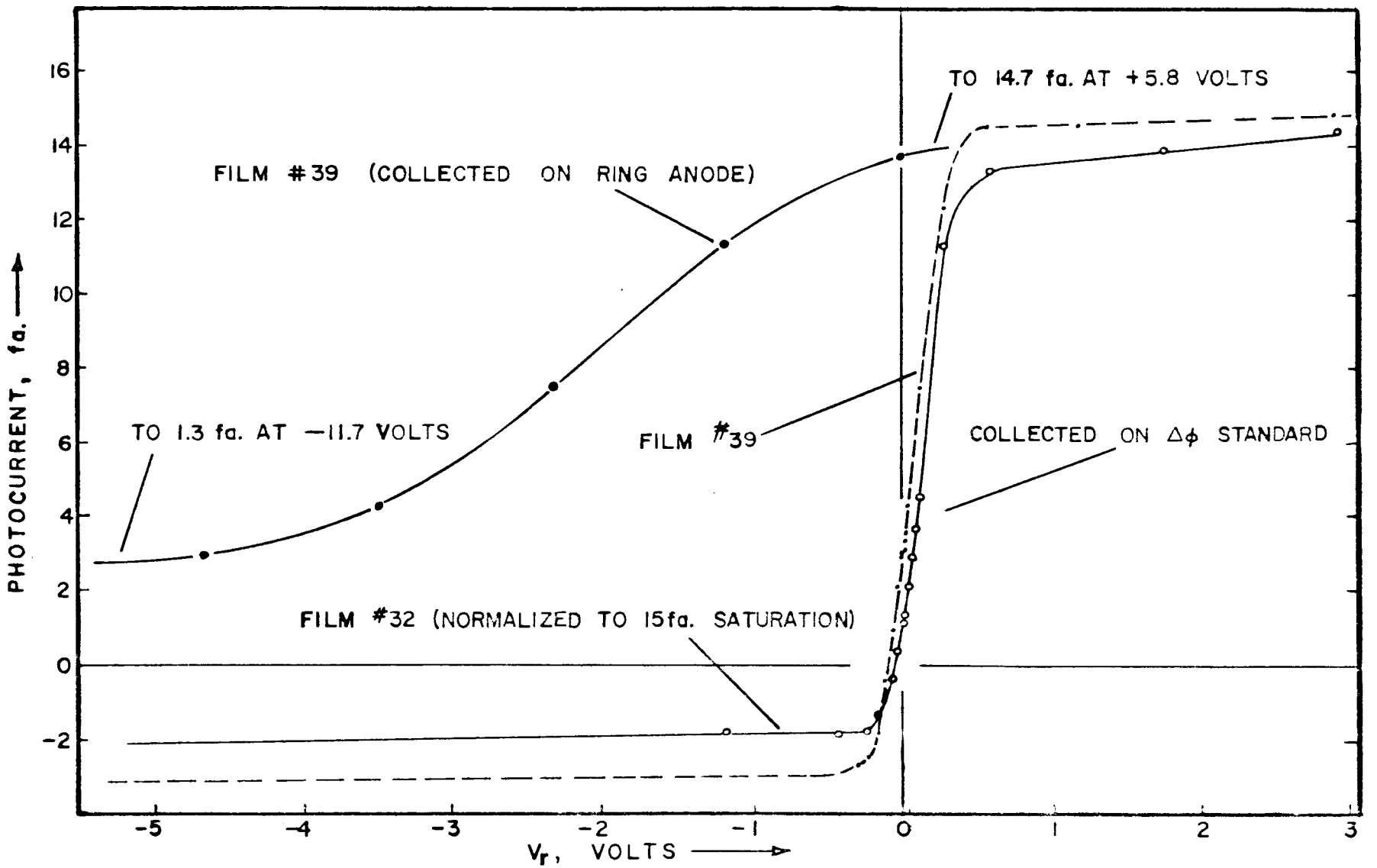

FIGURE 33. PHOTOCURRENT VERSUS RETARDING POTENTIAL

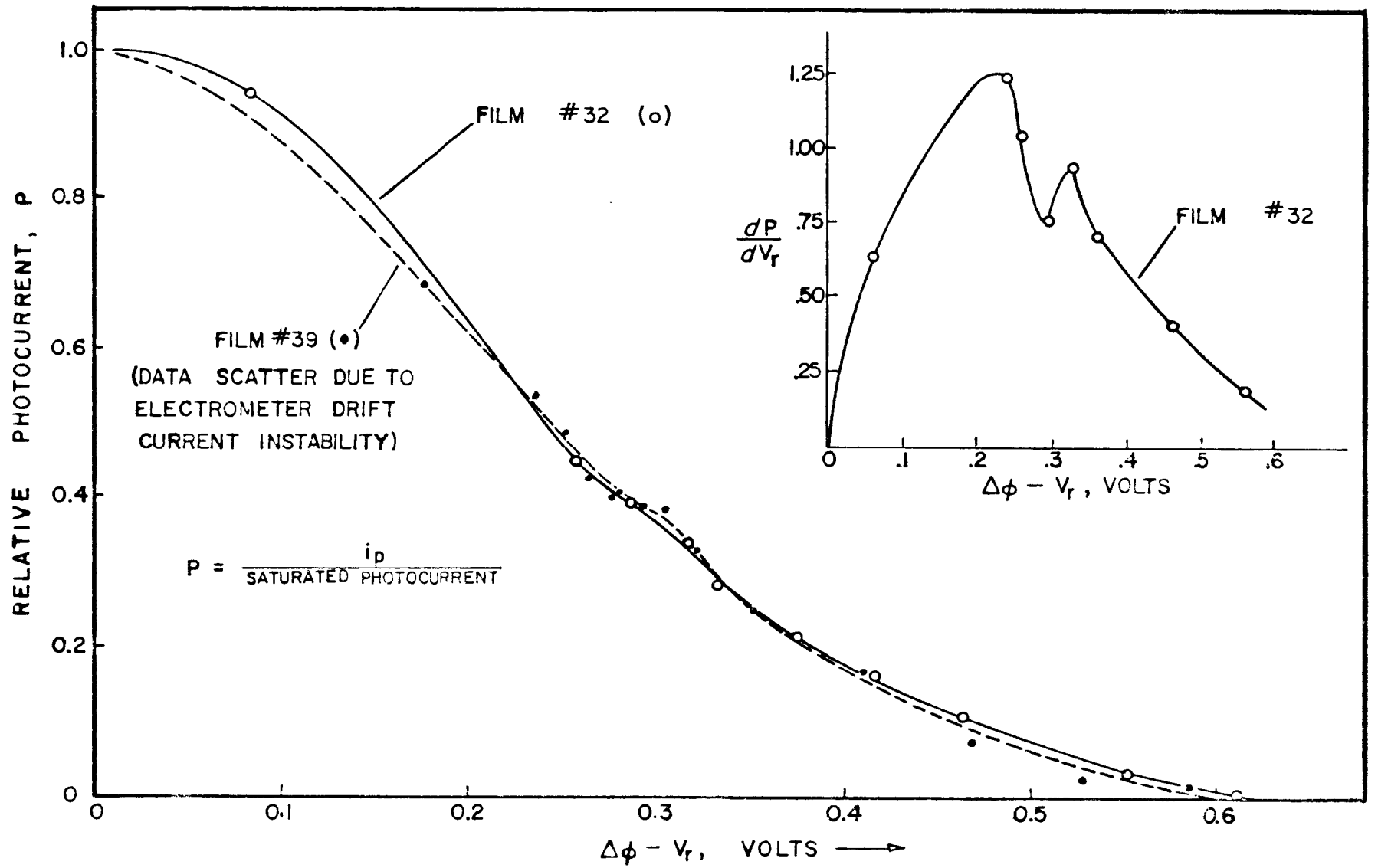

FIGURE 34. NORMALIZED i_p VERSUS V_r CURVES AND ENERGY DISTRIBUTION

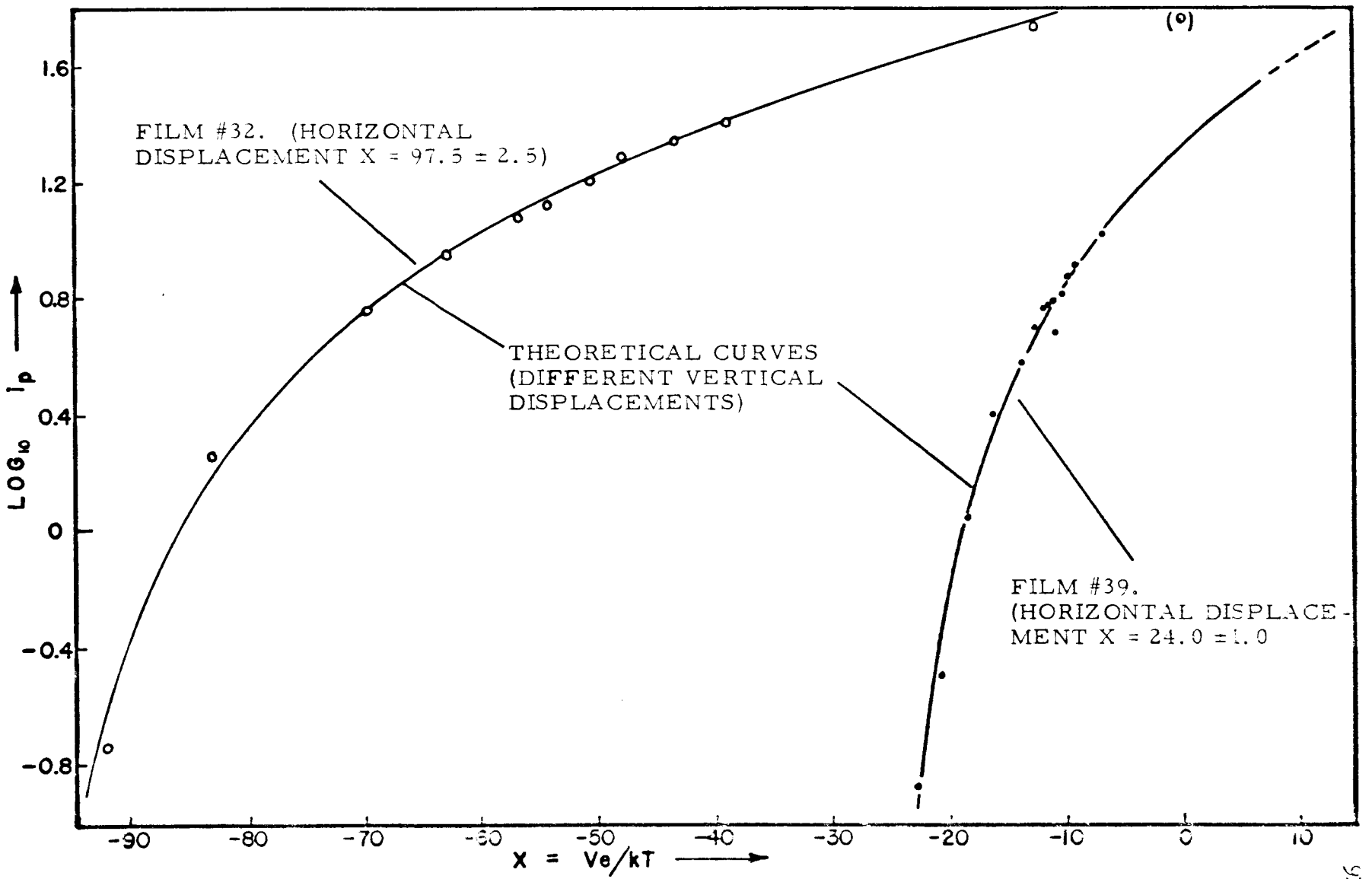

FIGURE 35. FOWLER-DUBRIDGE PLOTS

TABLE 4. WORK FUNCTION DATA FOR FILMS NO. 32 AND NO. 39

Film No.	32	39
T, ^{o}K	77	~ 300
V_m, volts	0.647 ± 0.016	0.613 ± 0.025
ϕe, volts[14]	4.36	4.40

In the Fowler-DuBridge data reduction the $i_p - V_r$ curves were shifted by an amount, $\Delta\phi$, (the observed value) which includes the real difference in work function, $\Delta\phi'$, plus thermoelectric potentials and the contact potential in the electrometer (~ 33 mv) so that the data plotted in Figurew 34 and 35 are completely corrected.

While the distribution curves appeared sensibly different in form for the two temperatures the work functions derived are essentially the same within experimental error but somewhat below handbook values (4.60 volts, reference 1).

While it is clear that more data would be required to fully define the energy distribution curves above there appears to be an interesting bump near V_r = 0.31 volts on both curves which may be due to band structure effects which have been observed by other workers (1).

---

14. $\frac{h\nu}{e}$ = 5.01 volts.

PHOTOCURRENT - THICKNESS ANALYSIS Using certain assumptions about the optical transmission and the electron mean-free-path within the metal it is possible to make an approximate model for the saturated photocurrent as a function of film thickness. This is a macroscopic theory, however, since it makes few assumptions about the actual crystal structure of the film or about the specific nature of electron scattering within the film.

Assume the following:

a) The film is two dimensional and is bounded by smooth, parallel planes. Although this assumption is poor for very thin films, we will be dealing with films greater than 160Å in thickness.

b) The probability of escape of an electron traveling a distance, x, to the film surface is given by:

$$P(x) = P_o e^{-x/L}$$

The electron mean-free-path, L, is considered constant over the narrow energy range involved and is assumed isotropic.

c) All photoelectrons have their velocities directed nearly normal to the surface. Since the velocity vector of most electrons must fall within a cone defined by apex angle, θ, defined by

$$\theta \leq \cos^{-1}\left(\frac{u_n}{u}\right) = \cos^{-1}\left\{\frac{E_f + \phi e}{E_f + h\nu}\right\} \qquad (39)$$

where u_n is the normal component of velocity necessary to overcome the work function, this approximation is good for this energy range ($\cos\theta \geq 0.977$).

If we assume photoemission to be a volume effect (using $e^{-x/s}$ to approximate the optical transmission of the film for convenience in integration over the film volume) then the current density, j_v, from the film (in light emergent geometry) is given by:

$$j_v = a_1[\exp(-\tau/s) - \exp(-\tau/L)]$$

where a_1 is a constant, τ is film thickness, and s is the optical absorption length. On the other hand, if we assume photoemission to be a surface effect the current density, j_s, for light emergent geometry is given by:

$$j_s = a_2[\exp(-\tau/x) + \exp(-\tau/L)]$$

In principle it would be possible to distinguish between a surface and volume effect from the shape of the photocurrent versus film thickness curves. However, for film thicknesses greater than about six electron mean-free-paths the curves given by the above expressions are experimentally indistinguishable (assuming L = 10 to 20Å and s = 100Å). Thus the late onset of conductivity (at a film thickness of 165Å) so limits the range of data as to make such a determination impossible for this experiment.

Therefore we assume a surface effect in accord with the Fowler-DuBridge theory.

Using a more accurate expression for the optical transmission of the film the surface effect current density is:

$$j_s = a_3 I_o \exp(-\tau/s) + a_4 I_o T_f \qquad (40)$$

where a_3 and a_4 are the emission coefficients for first and second sides of the film, I_o is incident light intensity, and T_f is the optical transmission of the film. Since we expect this expression to apply only at larger film thickness the contribution from the first surface becomes quite small for accepted values of electron mean-free-path (10-20Å) so photoemission should be proportional to optical transmission for relatively thick films. A plot of photocurrent versus optical transmission (λ = 2482Å) gives a good fit to such a relationship in the range 167Å and 219Å (in the range of stable properties at 77°K). When the film was raised to room temperature (No. 38) the situation clearly changes but data is insufficient to determine if Equation 40 no longer holds or if only a_4 has changed. (See Figure 36.) The latter assumption is plausible since the surface work function has changed with the temperature.

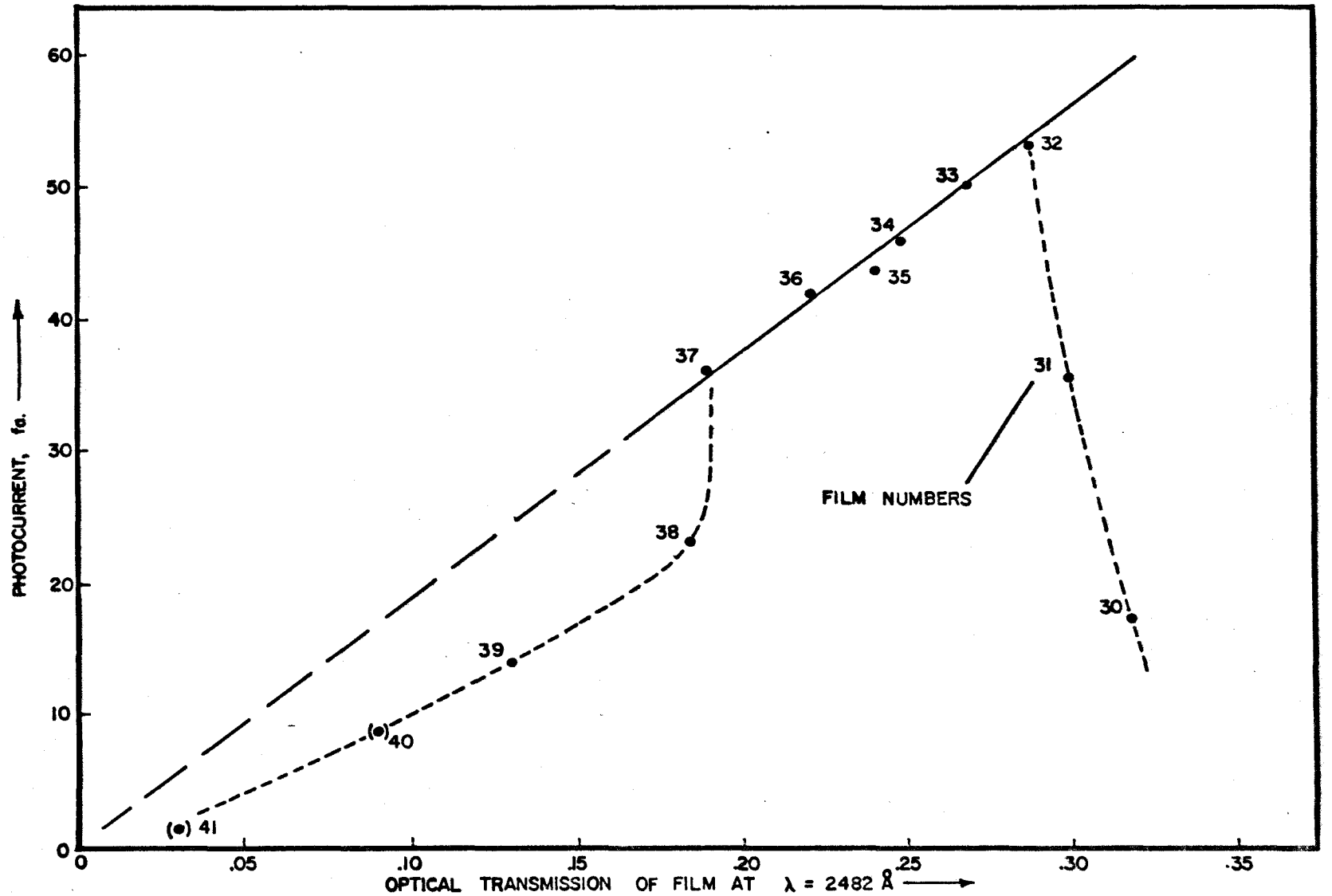

FIGURE 36. PHOTOCURRENT VERSUS OPTICAL TRANSMISSION

SUMMARY

The data of this experiment have demonstrated that the onset of electrical conductivity for antimony films deposited at 77°K occurs over a range of film thickness from 145 to 165Å, finally reaching a bulk value at 165Å. Three independent measurements indicated the onset of conductivity:

a) the increase in capacitance between the antimony and gold films,

b) the approach of contact potential values to reasonable, stable values, and

c) the onset of a stable, nonzero photocurrent.

All three measurements were in excellent agreement with each other and with the results of other workers (7, 22). By observing the transient charge transfer response to a voltage step the interelectrode capacitance method could, in principle, be used to obtain quantitative conductivity information.

The impetus provided by warming the film to room temperature makes it highly probable that a structural change began at film No. 30 changing the form from an amorphous, grainy state to a relatively smooth surfaced crystalline structure (16). The persistence of the amorphous structure to the large number of atomic layers indicated is reasonable considering the low deposition rate and the low surface energy at the substrate temperature used.

The photoemission and contact potential data analyzed by the Fowler-DuBridge method yielded 4.36 and 4.40 eV for the values of the work function at 77°K and at 300°K, respectively.

A macroscopic model for the variation of photocurrent with thickness (assuming a surface effect) fits the 77°K data well. The theory permits an electron mean-free-path of $\leq$ 40Å using the available data.

V. BIBLIOGRAPHY

1. Apker, L. E. Taft and J. Dickey. Some semimetallic characteristics of the photoelectric emission from As, Sb, and Bi. Physical Review 76:270-272. 1949.

2. Berglund, C. N. and W. E. Spicer. Photoemission studies of copper and silver: theory. Physical Review 136:A1030-A1044. 1964.

3. Berglund, C. N. and W. E. Spicer. Photoemission studies of copper and silver: experiment. Physical Review 136:A1044-A1064. 1964.

4. Brady, J. J. Energy distribution of photoelectrons as a function of the thickness of a potassium film. Physical Review 46:768-772. 1934.

5. Chopra, K. L. Influence of electric field on the growth of thin films. Journal of Applied Physics 37:2249-2254. 1966.

6. Condas, George A. Properties and preparation of thin antimony films of high uniformity. Review of Scientific Instruments 33:987-991. 1962.

7. Condas, George A. and Frederick O. Wooten. Properties of thin antimony films deposited in high vacuum. Journal of Applied Physics 32:323-324. 1961.

8. DuBridge, L. A. Theory of the energy distribution of photoelectrons. Physical Review 43:727-741. 1933.

9. Dushman, S. and J. M. Lafferty. Scientific foundations of vacuum technique. 2nd ed. New York, John Wiley and Sons, 1962. 806 p.

10. Einstein, Albert. Uber einen die Erzeugung und Verwandlung des Lichtes betroffen heuristischen Gesichtspunkt. Annalen der Physik 17:132-148. 1905.

11. Fowler, R. H. The analysis of photoelectric sensitivity curves for clean metals at various temperatures. Physical Review 38:45-56. 1931.

12. Herman, D. S. and T. N. Rhodin. Electrical conduction between metallic microparticles. Journal of Applied Physics 37:1594-1602. 1966.

13. Hughes, Arthur L. and Lee Alvin DuBridge. Photoelectric phenomena. New York, McGraw-Hill, 1932. 531 p.

14. Ives, H. E. The vectorial photoelectric effect in thin films of alkali metals. Physical Review 38:1209-1218. 1931.

15. Kane, Evan O. Theory of photoemission from semiconductors. Physical Review 127:131-141. 1962.

16. Learn, A. J. and R. S. Spriggs. Behavior of film conductance during vacuum deposition. Journal of Applied Physics 34:3012. 1963.

17. Makinson, R. E. B. The surface photoelectric effect. Physical Review 75:1908-1911. 1949.

18. McChesney, Evan W. Colorimetric micromethod for determination of antimony in biological materials. Industrial and Engineering Chemistry, Analytical edition 18:146-149. 1946.

19. Millikan, R. A. A direct photoelectric determination of Planck's "h". Physical Review 7:355-388. 1916.

20. Nordheim. L. W. The effect of the image force on the emission and reflexion of electrons by metals. Proceedings of the Royal Society, Ser. A, 121:626-639. 1928.

21. Penney, W. G. The photoelectric effect in thin metallic films. Proceedings of the Royal Society, Ser. A, 133:407-417. 1931.

22. Ruedy, J. E. Crystal structure and surface flow of thin evaporated antimony films. Physical Review 59:926. 1941.

23. Skinner, John George. The photoelectric current from the light emergent side of thin silver films as a function of thickness. Master's thesis. Corvallis, Oregon State College, 1958. 60 numb. leaves.